



ISBN 978-967-0194-52-3

PROCEEDINGS

Chemistry Undergraduate
Final Year Project Symposium

2014/2015

December 2015
Department of Chemistry, Faculty of Science
Universiti Teknologi Malaysia

© Department of Chemistry, Faculty of Science, UTM Johor Bahru.
Published by Department of Chemistry, Faculty of Science, UTM Johor Bahru
December 2015

ISBN 978-967-0194-52-3

All rights reserved. No part of this publication may be reproduced, copied, stored in any retrieval system or transmitted in any form or by any means – electronic, mechanical, photocopying, recording or otherwise; without prior permission in writing from the Head Department of Chemistry, Faculty of Science, Universiti Teknologi Malaysia, 81310 UTM Johor Bahru, Johor, Malaysia.

PROCEEDINGS

Chemistry Undergraduate Final Year Project Symposium 2014/2015

ADVISORY BOARD

Prof. Dr. Norsarahaida Binti Saidina Amin
Assoc. Prof. Dr. Zaiton Binti Abdul Majid

EDITORIAL BOARD

Prof. Dr. Hasnah Binti Mohd Sirat
Prof. Dr. Sugeng Triwahyono
Dr. Che Rozid Bin Mamat
Dr. Aemi Syazwani Binti Abdul Keyon
Dr. Siti Aminah Binti Sabtu@Setu
Dr. Nur Syafreena Binti Attan
Hashim Bin Baharin
Mohd Danial Bin Abdullah

TABLE OF CONTENT

CYCLOARTANE TYPE TRITERPENOID ISOLATED FROM THE LEAVES OF <i>BRUCEA JAVANICA</i> (L.) MERR <i>Nur Ain bt Abdul Halim and Shajarahtunnur bt Jamil</i>	1
HYDROGENATION KINETIC OF CARBON DIOXIDE USING MICROWAVE INDUCED ALLOYING Mo ₂ C AS CATALYST. <i>Hainorita Hairon and Abdul Rahim Yacob</i>	4
PROXIMATE NUTRIENT COMPOSITION OF <i>Chrysomya megacephala</i> AND <i>Chrysomya rufifacies</i> REARED ON BEEF SUBSTRATES <i>Nur Hazira Abdul Razak, Zainoha Zakaria and Naji Arafat Mahat</i>	13
GREEN SYNTHESIS OF THE FLAVOR ESTER BUTYL BUTYRATE CATALYZED BY NOVOZYME 435: A STATISTICAL APPROACH <i>Ida Nurhazwani Abd Rahman and Roswanira Abd Wahab</i>	21
STUDIES ON PHYTOCHEMICAL AND ANTIOXIDANT ACTIVITY OF THE FRUIT PEELS OF <i>LANSIUM DOMESTICUM</i> CORR. <i>Intan Syahira Ramli and Shajarahtunnur Jamil</i>	29
PRESENCE OF SELECTED ORGANOPHOSPHORUS PESTICIDE RESIDUES IN RAW CUCUMBER AND TOMATO SAMPLES IN TAMAN UNIVERSITI, JOHOR <i>Ling Sheau Jing and Naji Arafat Mahat</i>	32
PRODUCTION OF GERANYL PROPIONATE BY ADSORPTION OF <i>CANDIDA</i> <i>RUGOSA</i> LIPASE ON ACID FUNCTIONALIZED MULTI-WALLED CARBON NANOTUBES <i>Lok Yen Yen and Roswanira Abdul Wahab</i>	40
BIODEGRADABILITY AND ANTIMICROBIAL ACTIVITY OF CHITIN NANOWHISKERS-CHITOSAN FILMS <i>Nurul Faizah Binti Abd Ghapar and Zainoha Binti Zakaria</i>	47
GRAPHENE OXIDE DISPERSED WITH FERRITE NANO- PARTICLES AS MAGNETIC SOLID PHASE EXTRACTION ADSORBENT FOR CHLORPYRIFOS AND DIAZINON <i>Siti Fatimah binti Jamian, Wan Aini binti Wan Ibrahim and Hamid Rashidi Nodeh</i>	54
MODIFIED DESILICATED NATURAL ZEOLITE CATALYST FOR KNOEVENAGEL REACTION <i>Ainatul Mardiah Mat Rapi and Zainab Ramli</i>	63
CHEMICAL CONSTITUENTS AND ANTIOXIDANT ACTIVITY OF <i>GARCINIA</i> <i>PARVIFOLIA</i> MIQ. STEM BARK <i>Muhammad Aizam Hassan, Norazah Basar, Farediah Ahmad</i>	67
CHEMICAL CONSTITUENTS AND ANTIOXIDANT ACTIVITY FROM THE RHIZOMES OF <i>ZINGIBER CASSUMUNAR</i> <i>Nurul Amila Fadhlin Baharuddin and Hasnah Mohd Sirat</i>	71
PHOTODEGRADATION SCREENING ON CHLORPYRIFOS AND BENZOIC ACID USING TITANIA-BASED PHOTOCATALYST SUPPORTED ON PULASAN PEEL ACTIVATED CARBON <i>Anisaturrahmah Bt Mohd Yussof and Rusmidah Ali</i>	78

DEACETYLATION OF CHITIN ISOLATED FROM FERMENTED PRAWN WASTE TO PRODUCE CHITOSAN USING AUTOCLAVE METHOD <i>Zainoha Zakaria, Bong Tze Song, Marshifah Jamaludin</i>	85
FABRICATION OF <i>RHIZOMUCORMIEHEI</i> LIPASE REINFORCED NANOBIOCONJUGATES AS BIOCATALYSTS FOR A STATISTICALLY OPTIMIZED PRODUCTION OF EUGENOL BENZOATE <i>Fatin Myra Abd Manan dan Roswanira Abdul Wahab</i>	91
GENERATION OF PROTONIC ACID SITES FROM ALKANES OVER WO ₃ -ZrO ₂ EVIDENCED BY FTIR AND ESR SPECTROSCOPY <i>Asmida Kamarudin, Aishah Abdul Jalil and Sugeng Triwahyono</i>	99
DECOLORIZATON OF METHYLENE BLUE DYE USING MAGNETIC ANANAS <i>COMOSUS</i> LEAF <i>Siti Fairuz Ab Rashid, Zaiton Abdul Majid and Nursyafreena Attan</i>	105
SYNTHESIS AND BIOASSAY STUDIES OF BENZOXAZIN-4-ONE AND QUINAZOLIN-4-IMINE DERIVATIVES <i>Ng Choon Meng and Joazaizulfazli Jamalis</i>	112
DEMETALLIZATION OF TOXIC AND HEAVY METALS IN CLAM, <i>PAPHIA TEXTILE</i> UTILIZING CATALYTIC CHELATION TECHNIQUE <i>Nur Syafiqah Mohamad Sa'adan, Wan Azelee Wan Abu Bakar, Wan Nur Aini Wan Mokhtar</i>	117
DETERMINATION OF CHEMICAL COMPONENTS IN THE RHIZOMES OF <i>HEDYCHIUM CORONARIUM</i> <i>Siti Nazeerah Binti Kamarruddin and Hasnah Binti MohdSirat</i>	122
FERRITE-CALCIUM ALGINATE AS MAGNETIC SOLID PHASE EXTRACTION ADSORBENT OF COPPER(II) IONS IN WATER PRIOR TO FLAME ATOMIC ABSORPTION SPECTROSCOPY <i>Nur Syafika Shah Bania, Wan Aini Wan Ibrahima and Hamid Rashidi Nodeha</i>	126
KINETIC STUDY OF BIODIESEL USING EGG SHELL FOR BASE TRANSESTERIFICATION REACTION <i>Fatin Madihah binti Mamat and Abd Rahim Yacob</i>	133
ESSENTIAL OIL OF <i>PIPER BETLE</i> AND DERIVATIVES OF EUGENOL <i>Rafidah Binti Husain and Farediah Binti Ahmad</i>	140
THE EFFECT OF PH ON THE FORMATION OF NICKEL NANOSTRUCTURES BY CHEMICAL REDUCTION METHOD <i>Mohd Ridhwan bin Ramdzan and Che Rozid bin Mamat</i>	145
HYDRATION AND PROPERTIES OF BLENDED CEMENT SYSTEM INCORPORATING AEROGEL <i>Mohd Ikram Nul Hakim Bin Baharom and Che Rozid Bin Mamat</i>	153

DECOLORIZATION OF METHYLENE BLUE DYE USING MAGNETIC ANANAS COMOSUS LEAF

Siti Fairuz Ab Rashid, Zaiton Abdul Majid, and Nursyafreena Attan

Department of Chemistry, Faculty of Science, Universiti Teknologi Malaysia, 81310 Johor Bahru.

Abstract

The study was conducted to investigate the feasibility of using magnetic *Ananas comosus* leaf (MACL) as adsorbent for the removal of Methylene Blue (MB) dye. *Ananas comosus* leaf (ACL) was chosen due to the availability of this waste material. The ACL was first pretreated with different concentrations of nitric acid, HNO₃, to compare its surface area before modification process. Following that, ACL with the highest surface area was selected to produce MACL by precipitation of iron oxide on the surface of ACL. Both adsorbents, ACL and MACL were characterized using Fourier Transform Infrared Spectroscopy (FTIR), Brunauer-Emmett-Teller (BET), Scanning Electron Microscopy (SEM) and Energy Dispersive X-Ray (EDX). The BET surface area of ACL and MACL recorded are 35.20 m²/g and 81.42 m²/g respectively. Equilibrium and kinetic studies were carried out under different pH of MB solution, adsorbent dosage, contact time and initial MB concentration. The equilibrium data were fitted to Langmuir and Freundlich isotherms. The equilibrium adsorption for both ACL and MACL were best described by the Langmuir isotherm, with MACL exhibiting a larger adsorption capacity compared to ACL. The sorption data was also analysed using pseudo-first-order and pseudo-second-order kinetic model. The experimental data obtained was found to follow pseudo-second-order with correlation coefficient R² of 0.9889 and 0.9998 for ACL and MACL respectively.

Keywords: *Ananas comosus* leaf, methylene blue, kinetic model, equilibrium study

INTRODUCTION

Discharge of untreated or partially treated dye from industrial wastewater into the environment poses a serious threat and danger to life, not only by retarding the physicochemical and biological properties of environmental components but also from the toxicological point of view. Hence, the removal of synthetic dyes such as methylene blue is of great concern since some dyes and their degradation products may be carcinogens and toxic [1]. Methylene blue (MB), is a heterocyclic aromatic chemical compound, also known as Swiss blue [2]. Among the available technologies for dye removal from aqueous media, adsorption is widely studied because it is efficient, easy to operate, environment-friendly, and easy to disseminate. Adsorption technique is preferred compared to other techniques such as biodegradation, electrochemical degradation, photochemical degradation, coagulation/flocculation, sonicated degradation, membrane filtration, among others because adsorption has been found to be an efficient and economical process for the removal of pigments and other colorants and also to control the bio-chemical oxygen demand. However, of late, attention has been geared towards the application of magnetic particle technology to overcome environmental problems. The magnetic particles can be used to adsorb contaminants from aqueous or gaseous effluents and can be easily separated from the medium by a simple magnetic process after adsorption [4].

Adsorbent for the removal of MB from aqueous media was prepared from *Ananas comosus* leaf (ACL) or pineapple. The pineapple leaf is used in this study due to its availability in the pineapple industry. The production of magnetic *Ananas comosus* leaf (MACL) was carried out by precipitating iron oxide onto pretreated ACL. The characteristic of MB removal by ACL and MACL was analyzed by Langmuir and Freundlich adsorption isotherm through batch sorption experiment.

MATERIALS AND METHODS

Materials

The materials used for the study is ACL obtained from Pekan Nenas, Johor. Analytical grade sodium hydroxide pellet from Merck (99.5% purity), analytical grade Ferric chlorideferrous sulphate from Merck, nitric acid (Merck), ethanol and Methylene Blue from Sigma-Aldrich (M). The general chemical structure of Methylene Blue is illustrated in Figure 1.

Preparation and Characterization of ACL and MACL

The ACL were pre-treated by drying in an oven (80°C), ground and sieved (<75 µm) until fine powder was obtained. The ground ACL was treated using different concentration of nitric acid (HNO₃) i.e. 0.1 M, 0.5 M and

1.0 M for 24 hours. The magnetic ACL (MACL) was prepared by suspending 1.0 g ACL in 20 mL distilled water. A ferric chloride solution (FeCl_3) of 0.09 M was freshly prepared by adding 0.72 g of FeCl_3 into 52 mL distilled water. A ferrous sulphate solution, (FeSO_4) of 0.88 M was also prepared by adding 0.8 g FeSO_4 into 6 mL distilled water. Both solution were combined and vigorously stirred at 60-70°C. The suspension formed was added into an aqueous solution of ACL at room temperature and stirred slowly for 30 min. After mixing, 10 M NaOH was added dropwise into the suspension until the pH raised to 10-11. After mixing for 60 min, the suspension was aged at room temperature for 24 hours and then repeatedly washed with distilled water followed by ethanol. The MACL was vacuum filtered and dried overnight at 50°C in a hot air oven. The prepared ACL and MACL were characterized using BET Single Point Surface Analyzer, FTIR, XRD, XRF, FESEM-EDX, and SEM-EDX.

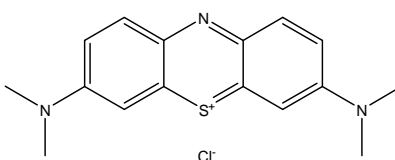


Figure 1: Chemical structure of MB dye

Batch Equilibrium Adsorption Study

Stock solution of MB was prepared by dissolving 0.1 g of MB into 1 L volumetric flask. The test solutions were prepared by diluting 1 mL, 1.5 mL, 2.0 mL, 2.5 mL and 3.0 mL are transferred into 100 mL volumetric flasks and diluted to series of 10 mg/L, 15 mg/L, 20 mg/L, 25 mg/L and 30 mg/L. A calibration curve was plotted using absorbance versus concentration of the solution to identify the concentration of MB solution after adsorption process.

The effect of ACL and MACL dose on the amount of MB adsorbed was obtained by contacting 100 mL of 50 mg/L MB solution with different amount of adsorbent. The amount of ACL and MACL used are in range of 0.1 to 1.0 g to see the effect of adsorbent dosage toward removal of MB.

The effect of pH on the removal of MB was analyzed under pH range 3-11. Experiments were conducted at 50 mg/L initial MB concentration for both 0.50 g ACL and MACL at 30 °C to observe whether pH is significant to the adsorption process.

A series of an appropriate concentration of 50 mg/L, 100 mg/L, 150 mg/L, 200 mg/L and 250 mg/L MB were prepared for quantifying the effect of initial MB concentration on adsorption rate with known amount of 0.50 g ACL and at a temperature of 30 °C.

RESULTS AND DISCUSSION

Characterization ACL and MACL

The FTIR spectra obtained revealed various functional groups on the surface of ACL and MACL. Based on the Table 1, some peaks were shifted or disappeared and new peaks were also detected. Iron oxide appeared at 473.17 cm^{-1} and 590.56 cm^{-1} at MACL indicates the presence of iron oxide onto ACL.

Table 1: FTIR data of ACL and MACL

Functional group	ACL	MACL
O-H (stretching)	3367.10	3402.67
C-H (stretching)	2918.43	2920.05
C=O	1737.83	-
C=C (aromatic)	1638.76, 1459.34	1633.17, 1419.95
N=O	1516.61, 1383.81	-
C-N	1338.22	1341.01
Iron oxide	-	473.17, 590.56

Absorbance in cm^{-1}

Surface area analysis (BET)

The surface areas of ACL and MACL treated with different concentration of nitric acid are shown in Table 2. The surface area analysis of ACL (35.20 m²/g) and MACL (81.42 m²/g) pretreated with 0.5 M HNO₃ shows the highest surface area .

Table 2: BET analysis of ACL and MACL

Sample	Surface area (m ² /g)
Raw ACL	7.69
ACL 0.1M HNO ₃	31.70
ACL 0.5M HNO ₃	35.20
ACL 1.0M HNO ₃	32.02
MACL 0.1M HNO ₃	69.80
MACL 0.5M HNO ₃	81.42
MACL 1.0M HNO ₃	65.52

Surface Morphology Analysis

Figure 1 (A-D) and Figure 1 (E-H) show the SEM micrograph of ACL and MACL at different magnification respectively. The ACL appears fibrous with the presence of agglomerates. The MACL surface shows the presence of pores. Precipitation of iron oxide onto surface of ACL plump out the agglomerated surface into a porous texture with iron oxide particles covering the pores. The distribution of pores are uniform. Pore development during iron oxide formation process enhanced the surface area of MACL compared to ACL.

Elemental Analysis

The elemental analysis of ACL and MACL are shown in Table 3. Elemental analysis of MACL shows the presence of iron attributed to the precipitation of iron oxide, confirming the precipitation of iron oxide on the ACL.

Table 3: Elemental analysis of ACL and MACL

Sample	Weight (%)				
	Carbon(C)	Oxygen(O)	Aluminium(Al)	Phosphorus (P)	Iron (Fe)
ACL	59.78	40.22	-	-	-
MACL	34.44	38.76	1.04	1.07	29.66

Adsorption Isotherm Study

Effect of dosage

The effect of adsorbent dosage on adsorption of MB onto ACL and MACL is illustrated in Figure 2. From the graph of ACL, the percent removal of MB increased from 48.63% to 85.07% from an increased in ACL dosage from 0.10 to 0.80 g. It was observed that the percent removal MB increased with increasing adsorbent dosage until to 0.80g ACL and gradually remains unchanged. The highest percentage removal of MB achieved using ACL was 85.07% and the optimum dose was found to be 0.80g for 100 mL of MB solution.

MACL displayed highest percent removal of MB up to 95.92%. The percent removal of MB using MACL increased rapidly using varies amount of MACL of 0.10 to 0.50 g which showed the percent removal of 90.56% to 95.92%. The graphs concluded that MACL promoted higher MB removal compared to ACL. These may be associated to the presence of iron oxide. For MACL, the optimum dose was 0.50 g with percentage removal of 95.92%.

Effect of solution pH

The effect of pH on the adsorption capacity of MB on ACL and MACL was studied by performing equilibrium adsorption experiments at different pH. Based on Figure 3, ACL shows the highest adsorption capacity at higher pH and achieve equilibrium at minimum pH 7. The adsorption capacity of MB increased up to pH 8 and remained nearly constant at pH 9 and above. Lower adsorption capacity of MB at acidic pH is due to the presence of excess H⁺ ions in the adsorbate which competes with cation groups on MB for adsorption site. A similar result was reported for adsorption of MB onto ACL and rejected tea [2][5].

Similarly, MACL also shows equilibrium adsorption capacity at a minimum pH 7. However, MACL displayed higher adsorption capacity compared to ACL. Both graphs exhibited increase in adsorption capacity at increase pH.

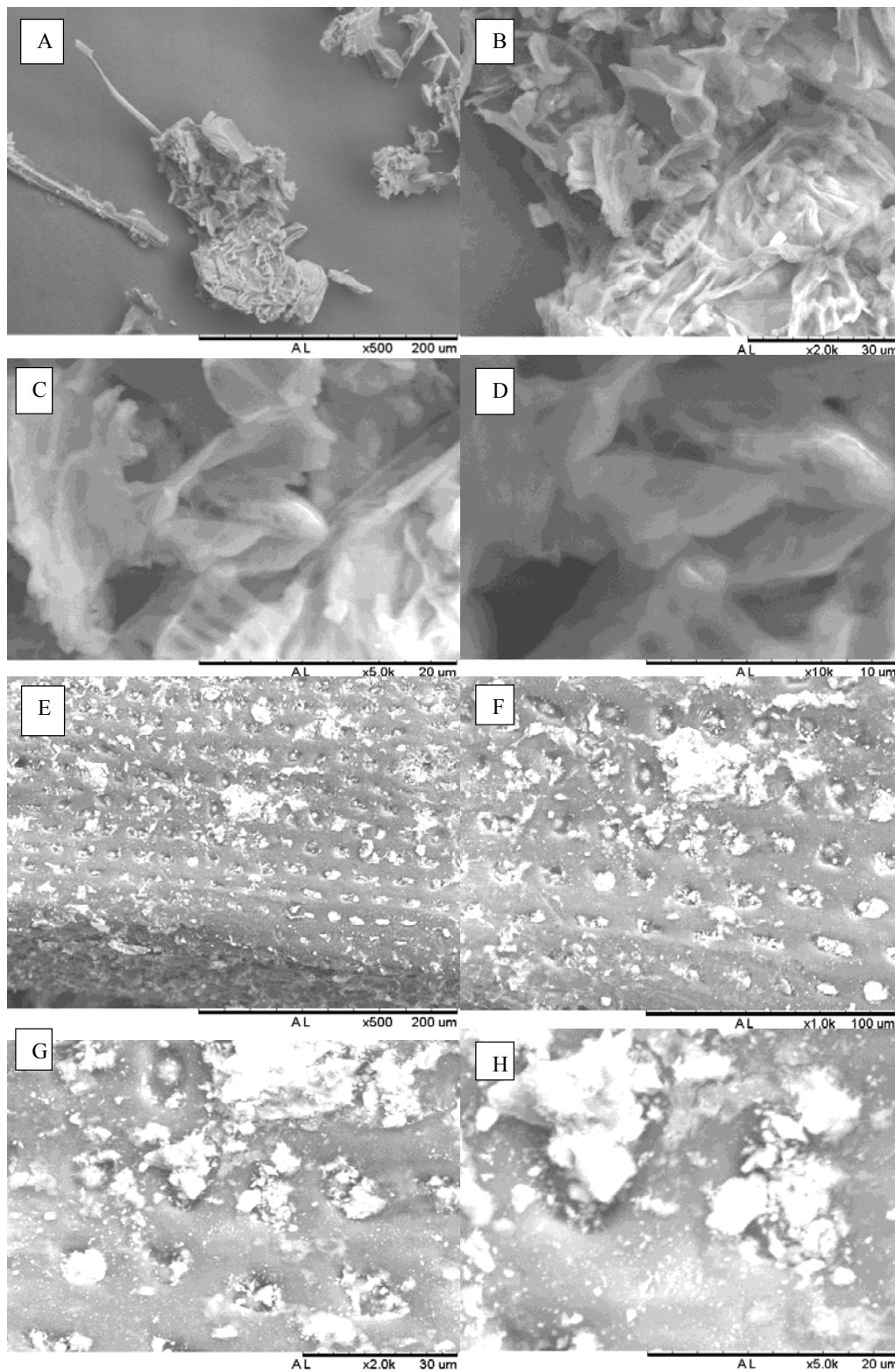


Figure 1 : SEM of ACL (A) x 500, (B) x 2.0k, (C) x 5.0k, (D) x 10.0k and MACL (E) x 500, (F) x 1.0k, (G) x 2.0k, (H) x 5.0k

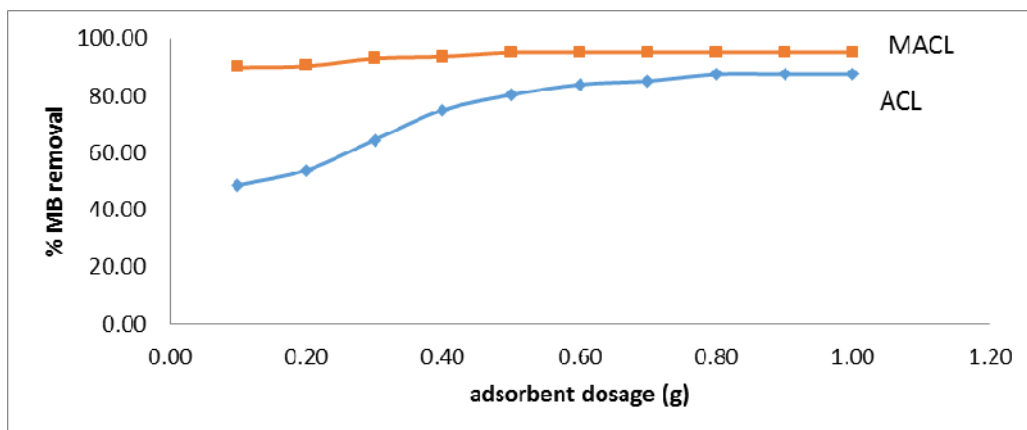


Figure 2: Effect of adsorbent dosage

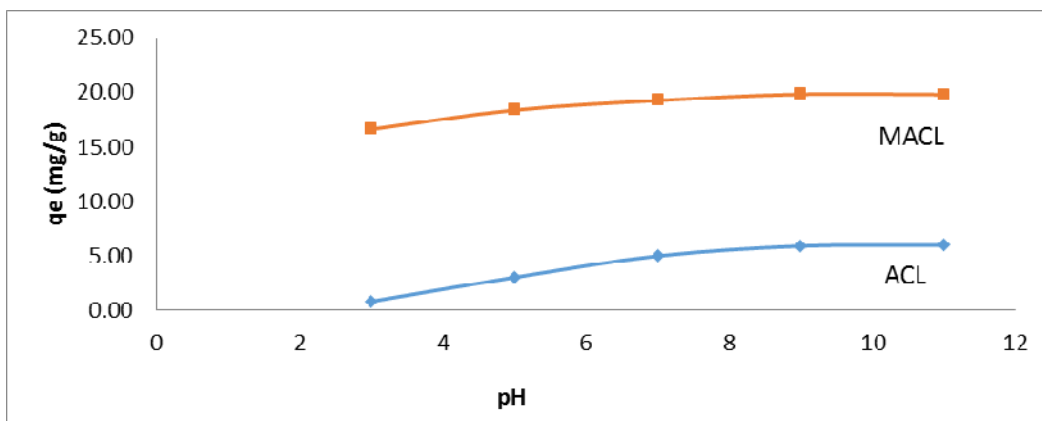


Figure 3: Effect of solution pH on adsorption of MB

Effect of initial concentration and contact time

Figure 4 shows the effect of initial dye concentration (50-250 mg/L) on the adsorption of MB. For ACL, it was observed that amount of MB adsorbed was rapid for the first 40 minutes and proceeded gradually at slower rate and finally reached saturation at 90 minutes for 50 mg/L. The equilibrium adsorption increases from 5.90 to 21.3 mg/g with concentration of 50 to 250 mg/L. It was found out that equilibrium removal of MB decreased from 88.0% to 68.4% as concentration increased from 50 to 250 mg/L. MACL shows rapid adsorption for the first 25 minutes and reached equilibrium at 30 minutes for 100 mg/L.

Equilibrium Study

Based on the Table 4, value of q_{max} for ACL is lower compared to MACL. MACL shows higher maximum adsorption capacity of 70.92 mg/g. This results from the higher surface area of MACL compared to ACL. Moreover, iron oxide also plays an important part as active site in MB removal. R^2 value is an indication to determine the favourability of adsorption. From the value of coefficient correlation R^2 , both ACL and MACL exhibit $R^2 > 0.99$. This means that Langmuir isotherm is more favourable.

Table 4: Langmuir isotherm parameter

Sample	q_{max} (mg/g)	K_a (dm ³ /mg)	R^2
ACL	30.769	0.034	0.9937
MACL	70.92	0.091	0.9942

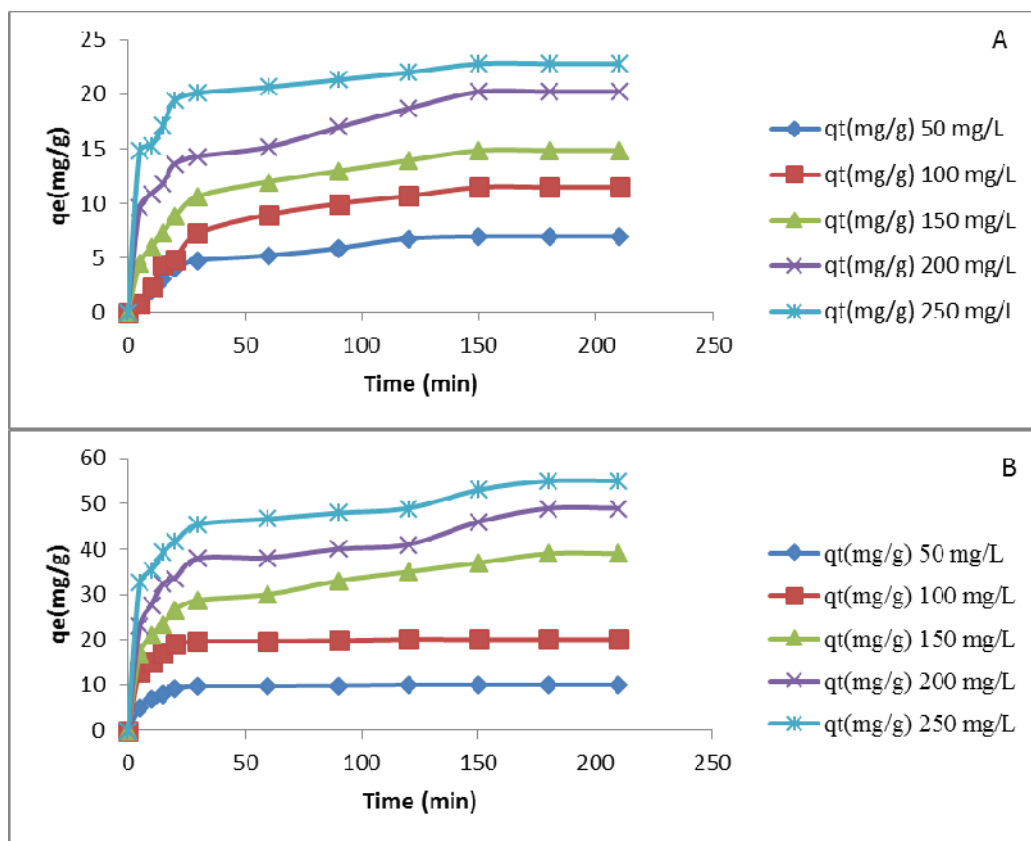


Figure 4: Effect of contact time and initial concentration on the adsorption of MB on (A) ACL and (B) MACL

Table 5: Freundlich isotherm parameter

Sample	K_F	$1/n$	R^2
ACL	1.090	0.8614	0.8957
MACL	4.500	1.0471	0.9566

Multilayer adsorption is best described by Freundlich isotherms where only employed onto heterogeneous surface. The Freundlich isotherm for ACL and MACL parameters were tabulated in Table 5. There are two Freundlich constants which are K_F and n . K_F is known as adsorption or distribution coefficient that show the quantity of dye adsorbed for a unit equilibrium concentration. $1/n$ indicates the surface heterogeneity. The adsorption is said heterogeneous when value of n closer to zero [6]. From the $1/n$ values above, the adsorption of ACL and MACL are homogeneous as the $1/n$ values are further than zero. R^2 value for both ACL and MACL are 0.8957 and 0.9566.

Thus, in brief the adsorption follows Langmuir isotherms as R^2 value higher than Freundlich. It can be concluding that the adsorption involved only monolayer coverage which focusing on chemical adsorption.

Kinetic study

Table 6 indicated that the kinetic data did not fit well with pseudo-first-order. The R^2 results from pseudo-first-order are rather low which are 0.6353 and 0.9156 for ACL and MACL. The q_e experimental and q_e calculated gave a big different hence the adsorption of MB onto ACL and MACL does not follow pseudo-first-order kinetic.

The plot of t/q_t against t as in Figure 6 shows that the intercept are very close to zero. This means that the pseudo-second-order is more applicable and favourable. The coefficient correlation, R^2 for pseudo-second-order is $R^2 > 0.98$ for both ACL and MACL. Since the q_e calculated and q_e experimental of pseudo-second-order displayed the almost same value, the kinetic studied is more suitable and applicable to pseudo-second-order.

Table 6: Kinetic parameters

Sample	Pseudo-first-order				Pseudo-second-order		
	q _e exp (mg/g)	q _e cal (mg/g)	k ₁ (1/min)	R ²	q _e cal (mg/g)	k ₂ (1/min)	R ²
ACL	30.76	14.64	0.030	0.6353	25.19	0.005	0.9889
MACL	70.92	24.15	0.023	0.9156	76.92	0.006	0.9998

CONCLUSION

Based on adsorption study, the adsorption capacity obtained for ACL and MACL are 30.77 mg/g and 70.92 mg/g respectively. Based on R² values which are 0.9937 for ACL and 0.9942 for MACL, the adsorption could be fitted to the Langmuir isotherm. Kinetic studies shows that the adsorption is pseudo-second-order with R² values for ACL is 0.9889 and MACL 0.9998.

REFERENCES

1. Weng C.H., Lin Y.T., Tzeng T.W. (2009). Removal of methylene blue from aqueous solution by adsorption onto pineapple leaf powder, *Journal of Hazardous Materials*, **170**, 417–424
2. Chen, M.C., Wu, J.Y., Huang, C.C., Liang, Y.M. and Hwang, S.C.J. (2003) Decolourization of azo dye using PVA-immobilized microorganisms, *J. Biotechnol*, **101**, 241–252.
3. Rakesh Kumar Ghosh, D. Damodar Reddy. (2013). Tobacco Stem Ash as an Adsorbent for Removal of Methylene Blue from Aqueous Solution: Equilibrium, Kinetics, and Mechanism of Adsorption, *Water Air Soil Pollut* 224:1582, 1-12
4. Luiz C.A. Oliveira et.al. (2002). Activated carbon/iron oxide magnetic composites for the adsorption of contaminants in water, *Carbon* 40, 2177-2183
5. Nasuha N, Hameed B.H., Azam T. Mohd Din. (2010). Rejected tea as a potential low-cost adsorbent for removal of methylene blue, *J. Hazard. Mater*, **175**, 126-132
6. Zhen, C., Wei, M. and Mei, H. (2008). Biosorption of Nickel and Copper onto treated alga (undaria pinnatifida): Application of isotherm and kinetic models. *Journal of Hazardous Materials*. **155**. 327-333

SYNTHESIS AND BIOASSAY STUDIES OF BENZOXAZIN-4-ONE AND QUINAZOLIN-4-IMINE DERIVATIVES

Ng Choon Meng and Joazaizulfazli Jamalis

Department of Chemistry, Faculty of Science, Universiti Teknologi Malaysia, 81310 Johor Bahru.

Abstract

The 4*H*-3,1-benzoxazin-4-one and quinazolin-4-imine derivatives have been synthesized in simple and one step reaction. The reaction of anthranilic acid and benzoyl chloride, terephthaloyl dichloride and 4-chlorobenzoyl chloride in pyridine yielded 2-phenyl-4*H*-3,1-benzoxazin-4-one (78.91%), 1,4-(di-4*H*-3,1-benzoxazin-4-one)benzene (55.23%) and 2-(*p*-chlorophenyl)-4*H*-3,1-benzoxazine-4-one (33.20%) respectively. The benzoxazin-4-one derivatives were then treated with hydrazine hydrate in absolute ethanol to form 2-phenylquinazolin-4-imine (70.90%), 1,4-(diquinazolin-4-imine)benzene (43.70%) and 2-(*p*-chlorophenyl)quinazolin-4-imine (35.81%). The resulting compounds were characterized using ATR and ¹H NMR using CDCl₃ as solvent. From both spectra it showed that the synthesis of targeted compound, 4*H*-3,1-quinazolin-4-one was unsuccessful. The resulting compounds after treated with hydrazine hydrate were proposed to be quinazolin-4-imine compounds based on the data analyzed from ATR and ¹H NMR spectrum. Antioxidant test using DPPH free radical scavenging has been carried out on the six compounds synthesized. The results showed that 4*H*-3,1-benzoxazin-4-one derivatives did not show antioxidant activity while the compounds of quinazolin-4-imine derivatives showed good antioxidant activity as the IC₅₀ value obtained are lower than positive control of ascorbic acid except for 1,4-(diquinazolin-4-imine)benzene. Among the quinazolin-4-imine derivatives, 2-phenylquinazolin-4-imine showed the highest antioxidant activity at IC₅₀ value at 2.66ppm. The introducing of electron withdrawing group at phenyl substituent was found to reduce ability of compounds in antioxidant activity.

Keywords: Heterocycle, synthesis, 4*H*-3,1-benzoxazin-4-one, quinazolin-4-imine, antioxidant

INTRODUCTION

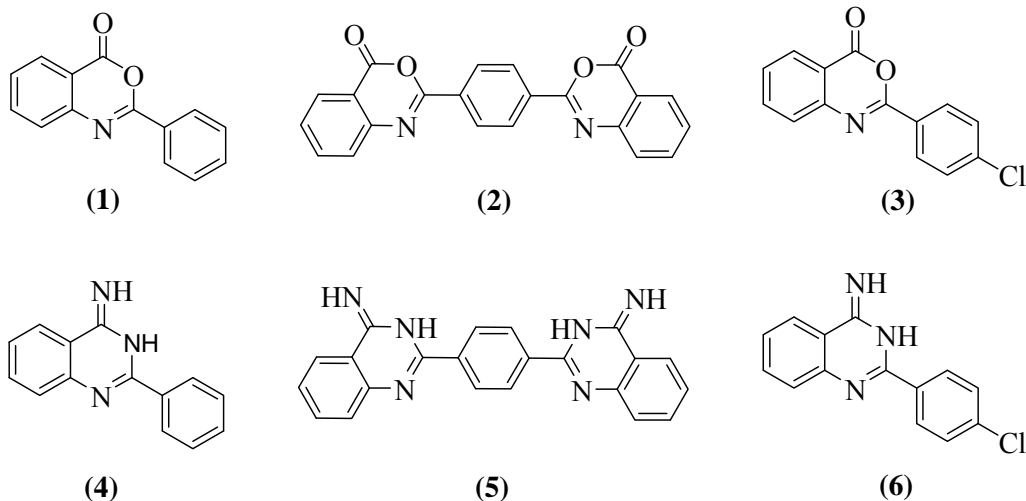
Benzoxazinone belongs to the group of heterocyclic compounds that consist of unsaturated six-membered rings with two heteroatoms of oxygen and nitrogen. While the quinazoline consist of unsaturated six-membered rings with two heteroatoms of nitrogen. Heterocyclic compounds are commonly become an interest in pharmaceuticals and agrochemical industries due to their natural occurrence [1]. Numerous additives and dyes used in industrial application such as cosmetic are heterocyclic in nature. The common biological activities possessed by synthetic heterocyclic compounds are antibacterial [2], antifungal [3], anti-inflammatory [4] and antioxidant [5]. The wide range of biological activities possessed by heterocycles is mainly due to the extraordinary wide range of reaction of the compounds. Heterocyclic can behave as either acid or base to form anion or cation depending on the pH value of the medium. Besides, some heterocyclic easily interact with electrophilic reagent while some with nucleophiles, or both. Some can be easily oxidized but reduction resistant, or vice versa. Furthermore, there are heterocyclic compounds which simultaneously demonstrate all of the mentioned properties.

Benzoxazinone can exist in various types depends on the position of keto group. The keto group may occur at either position two, four or both [6]. The keto group also may occur at position three of the structure such as natural occurring of benzoxazinone in maize and wheat [7]. Among all the types of benzoxazinone and quinaozoline, 4(3*H*)-benzoxazinone and quinazolinone are more prevalent to be used as intermediates of drugs synthesis or as natural products in biosynthetic pathway. This is partly because of its structure possess wide range of reaction and being derived from anthranilates with various esters, isotoicanhydride and anthranilamide. In this paper, we report the synthesis and characterization of 4*H*-3,1-benzoxazin-4-one and quinazolin-4-imine compounds (**1-6**). In addition, all the compounds were evaluated for their antioxidant activity using DPPH radical scavenging.

EXPERIMENTAL

Thin layer chromatography (TLC) analysis was conducted by using thin aluminium plate of Merck Silica gel 60F254 of 0.2 mm thickness. The spots on TLC were visualized using Ultraviolet at 254nm and 365nm. The purification of compound was carried out by column chromatography using Merck Silica gel and the eluent used was mixture of hexane acetone in the ratio of 40:60. The products were characterized by using ATR and ¹H NMR. Sample product was measured on Attenuated Total Reflectance (ATR) with 20 scans for each sample at a resolution of 4cm⁻¹ per measure. The IR spectra was recorded on PerkinElmer FT-IR Spectrometer Frontier. The ¹H spectra were obtained using 300MHz spectrometer for benzoxazinone and 400MHz spectrometer for

quinazoline and the chemical shift were reported in ppm using CDCl_3 as solvent. The ^1H NMR spectra was recorded at 300 MHz and 400 MHz using Bruker Avance Spectrophotometer.



ORGANIC MATERIALS

Starting material used was anthranilic acid which was purchased from Sigma-Aldrich. The derivatives of acyl chloride of benzoyl chloride, terephthaloyl dichloride and 4-chlorobenzoyl chloride were purchased from Tokyo Chemical Industry CO., LTD in December 2014.

SYNTHESIS AND CHARACTERIZATION

Benzoyl chloride (10.00mmol) was added into anthranilic acid (1.03g, 7.50 mmol) and pyridine (30 mL) separately. The mixture was then refluxed for 3 hours and the reaction was monitored under thin layer chromatography (TLC). The spots on TLC were visualized under UV light. Upon the reaction was completed, the reaction mixture was cooled and then poured into cooled diluted hydrochloric acid (15mL). The solid was filtered and recrystallized from ethanol. The synthesis method is repeated by replacing terephthaloyl dichloride (1.00g, 7.3mmol) and 4-chlorobenzoyl chloride (1.00g, 7.3mmol). The compound synthesized from terephthaloyl dichloride(2) is further purified by silica gel-60 column chromatography and mixture of hexane-acetone in 40:60 ratio. The compound (1) was obtained is a white solid (1.33 g, 78.91%). Compound (2) obtained as yellow solid (0.74 g, 55.23%), compound(3) appeared as white solid (0.62g, 33.20%). The 4*H*-3,1-benzoxazin-4-one derivatives synthesized were subjected to characterize by using ATR and ^1H NMR. The confirmed compounds were used for the synthesis of the corresponding quinazolin-4-imine derivatives.

A mixture of 2-phenyl-4*H*-3,1-benzoxazin-4-one (0.30g, 1.34mmol)(1) and hydrazine hydrate (64%, 2.00mmol) was refluxed in ethanol (30 mL) for 4 hours. The reaction was monitored under thin TLC. The spots on TLC were visualized under UV light. Upon the reaction was completed, the reaction mixture was cooled and poured into cooled distilled water (20 mL). The mixture was then concentrated and filtered off the solid. The separated solid was recrystallized from ethanol. The synthesis method was then repeated by replacing 2-phenyl-4*H*-3,1-benzoxazin-4-one with 1,4-(Di-4*H*-3,1-benzoxazin-4-one)benzene (0.10g, 0.39mmol)(2) and 2-(*p*-chlorophenyl)-phenyl-4*H*-3,1-benzoxazin-4-one (0.10g, 0.35mmol)(3). The compound (4) was obtained as a white solid (0.41 g, 70.90%). Compound (5) obtained as yellow solid (0.34 g, 43.70%), compound (6) appeared as white solid (0.03 g, 35.81%).

The six compounds synthesized were used to carry out antioxidant testing. The method in determination of antioxidant activity was referring to the method used by Fu. R. *et al* in their previous research [8]. Each sample was dissolved in methanol to prepare 1000 ppm of sample solution. The stock solution was then diluted to 800ppm, 600ppm, 400ppm, 200ppm, 100ppm, 80ppm, 60ppm, 40ppm, 20ppm, 10ppm, 5ppm and 1ppm. The purple solution of 2,2-diphenyl-1-picrylhydrazyl, DPPH was prepared by dissolve DPPH (3.94 mg) in methanol (100mL) in a dark container covered with aluminium foil. Ascorbic acid was used as the positive control. Each sample solution of different concentration (100 μL) was added into the sample well together with the DPPH

solution (100 μ L) and methanol (100 μ L) for blank sample separately. Triplicate samples were used for each sample with different concentration. The mixtures were then incubated at 25°C for 30min, and the absorbance at 517nm was measured using microplate reader. The radical scavenging activity was calculated using equation as follow:

$$\text{radical scavenging activity (\%)} = \left[1 - \frac{(A_i - A_r)}{A_c} \right] \times 100$$

Where A_c is the absorption of the negative control, A_i is the absorbance of the experimental group and A_r represents the background absorption.

RESULTS AND DISCUSSION

Compound (**1**) was obtained from the recrystallization appeared as a white solid (1.33 g, 78.91%). The ATR spectrum of compound (**1**) is in agreement with the research conducted before [8]. The ATR spectrum showed a stretching peak for C-H bond of aromatic is observed above 3000 cm^{-1} and was typically showed as a multiplicity of weak band due to the present of more than one benzene system in the structure. The stretching of C=O bond was observed as a strong band at 1762 cm^{-1} which is slightly higher than the theoretical value of normal ester compound. The increase in intensity and wavenumber were caused by the conjugation with the ester single bonded-oxygen. The lone pair electron on oxygen atom donated to form a temporary C=O bond causes the oxygen atom to be more positive. This causes the electron deficiency in oxygen atom and results in the pulling of electron from C=O ester by inductive effect. The C=N stretching mode is observed at wavenumber of 1610 cm^{-1} as studied by previous research [9]. The stretching of C=N bond at lower wavenumber is due to the conjugate effect of C=C from the phenyl group attached at position two of the benzoxazinone skeleton. The C=C aromatic absorption peaks are observed at 1572 cm^{-1} and 1474 cm^{-1} . Analysis of the ^1H NMR spectrum showed that all proton of benzoxazinone exhibited a low field signal started from 7.5ppm. The most low field signal δ 8.33 ($J=7.2\text{Hz}$) belongs to hydrogen located at *ortho*-position of the phenyl substituent, H_o which was subjected to the electrostatic field effect from lone pair electron of nitrogen [10]. The proton in fifth position, H_5 showed signal at δ 8.26 ($J=7.8\text{Hz}$, 0.9Hz) which is low field than H_6 to H_8 due to the electron deshielded by an anisotropic effect of the *peri*-carbonyl at the fused ring. H_7 and H_8 were observed at δ 7.85 ($J=7.8\text{Hz}$, 0.9Hz) and δ 7.71 ($J=7.8\text{Hz}$). The remaining protons were observed at δ 7.49-7.61 (4H).

Compound (**2**) obtained was appeared as yellow solid (0.74g, 55.23%) after recrystallization and purification using silica gel column. The ATR spectrum showed absorption peak similar to compound (**1**) where 3040 cm^{-1} belongs to C-H aromatic, 1763 cm^{-1} was C=O ester, 1694 cm^{-1} was C=N, 1612 and 1474 cm^{-1} for C=C aromatic. From the ^1H NMR spectrum, the low field peak was the peak of *ortho*-position proton, H_o at δ 8.50. This peak represented four protons from the phenyl substituent without splitting as the protons are identical to each other by symmetry [11]. These protons would give only a single NMR peak since they have the same chemical shift. The other protons at the fused ring exhibited similar chemical shift and splitting with the compounds (**1**), which peaks at δ 8.31 for H_5 ($J=7.4\text{Hz}$), H_7 at δ 7.90 ($J=7.4\text{Hz}$), H_8 at δ 7.78 ($J=7.4\text{Hz}$) and H_6 at δ 7.60 ($J=7.4\text{Hz}$). Compound (**3**) obtained is a white solid (0.62 g, 33.20%). Both ATR and ^1H NMR spectrum showed similar peak as observed in compound (**1**) except for the absence of H_p in ^1H NMR since the H_p in (**3**) had been replaced by the chlorine atom. The ATR spectrum of (**3**) showed absorption peak at 1769 cm^{-1} for C=O ester, 1622 cm^{-1} for C=N, 1604 cm^{-1} and 1489 cm^{-1} for C=C aromatic. ^1H NMR spectrum showed peaks at δ 8.27 for both H_o and H_5 , δ 7.85 for H_7 ($J=7.8\text{Hz}$, 1.2 Hz), δ 7.70 H_8 ($J=7.8\text{Hz}$) and δ 7.54 for both H_m and H_6 .

For the condensation process of 4*H*-3,1-benzoxazin-4-one with hydrazine hydrate, the targeted compound synthesis was the 3-amino-2-substituted-4*H*-3,1-quinazolin-4-one derivatives as reported previously [12]. However, from the ATR and ^1H NMR obtained, the proposed structure of compounds synthesized was quinazolin-4-imine derivatives. Compound (**4**) obtained as a white solid (0.21g, 70.90%). From the ATR, the C=O stretching did not observe in compound (**4**) and a peak was observed at 1649 cm^{-1} was believed to belong to C=N. Besides, the N-H stretching peak at 3318 cm^{-1} also observed in the ATR. Other than that, two peaks which were 1603 cm^{-1} and 1449 cm^{-1} also observed for C=C aromatic. From the ^1H NMR, a N-H peak was observed at δ 11.88 and it was believed to come from N-H at position 3 that resembled to the compound of 2-phenyl-4*H*-3,1-quinazolin-4-one as reported in other research [14]. Therefore it is further proven that the solid formed was a quinazolin-4-imine derivative. The proton at the fused ring, H_5 was found to shift to lower field at δ 8.83 ($J=7.7\text{Hz}$) as compare to the H_5 in (**1**). The H_o was observed at δ 8.06 ($J=6.8\text{Hz}$), H_6 at δ 7.12 ($J=7.7\text{Hz}$) and the remaining six proton were observed in the δ 7.63 to 7.12.

Compound (**5**) was obtained as a yellow compound (0.24g, 43.70%). From the ATR, the N-H stretching was observed at 3351 cm^{-1} , followed by C=N stretching at 1666 cm^{-1} . The C=C aromatic stretching were observed at 1587 cm^{-1} and 1446 cm^{-1} . The ^1H NMR spectrum was similar to compound (**1**), where the N-H peak was observed at δ 12.44, followed by H_5 at δ 8.83 ($J=7.6$ Hz). The *ortho*position proton, H_O was observed at δ 8.25 ($J=7.0$ Hz), H_8 at δ 7.92 ($J=7.6$ Hz), H_7 at δ 7.61 ($J=7.6$ Hz) and H_6 at δ 7.22 ($J=7.6$ Hz). The N-H from imine was observed at δ 8.16 ($J=7.0$ Hz). Compound (**6**) appeared as a white (0.23g, 35.81%). From the ATR, the N-H stretching was observed at 3319 cm^{-1} , followed by C=N stretching at 1668 cm^{-1} . The C=C aromatic stretching were observed at 1600 cm^{-1} and 1451 cm^{-1} . The ^1H NMR spectrum showed the peak of N-H at δ 11.97, followed by H_5 at δ 8.82 ($J=7.7$ Hz). The *ortho*position proton, H_O was observed at δ 8.00 ($J=8.4$ Hz), H_8 , H_7 , H_m , and imine N-H were observed as multiplet peak at δ 7.46 - 7.61. The H_6 was observed at δ 7.15 ($J=7.7$ Hz).

The antioxidant activity of benzoxazinone and quinaozolin-4-imine was tested using 2,2'-diphenyl-1-picrylhydrazyl (DPPH). From the results obtained, it clearly shows that the compounds of 4*H*-3,1-benzoxazin-4-one derivatives do not possess any antioxidants activities after incubation of 30 mins with DPPH. The negative results of the antioxidant activities from 4*H*-3,1-benzoxazin-4-one can be explained by the lack of free hydrogen atom to be donate and stabilize the free radical DPPH. The compounds of all quinazolin-4-imine synthesized possess good antioxidant activities even at low concentration of 100ppm. The capability in antioxidant is due to the active hydrogen at the nitrogen atom of the quinazolin-4-imine skeleton. The IC_{50} of compound (**4**), (**5**) and (**6**) were 2.66ppm, 28.40ppm and 8.04 ppm respectively. From the IC_{50} values, it was concluded that the introducing of chlorine atom at *p*-position of phenyl group slightly reduced the ability of the compound due to the inductive effect.

CONCLUSION

A series of 2-substituted-4*H*-3,1-benzoxazin-4-one and quinazolin-4-imine compounds had been synthesized with a simple and single step method by using anthranilic acid as starting material. The benzoxazin-4-one compound derivatives synthesized are 2-phenyl-4*H*-3,1-benzoxazin-4-one (**1**) (78.91%), 1,4-(di-4*H*-3,1-benzoxazin-4-one)benzene (**2**) (55.23%) and 2-(*p*-chlorophenyl)-4*H*-3,1-benzoxazine-4-one (**3**) (33.20%). In the synthesis of the quinazolin-4-one derivatives, the desired product is not obtained. Instead of quinazolin-4-one is synthesized, the unexpected products synthesized were proposed to be the quinazolin-4-imine derivatives based on the data analysis from ATR and ^1H NMR spectrum obtained. Therefore in the study, the quinazolin-4-imine derivatives obtained are 2-phenylquinazolin-4-imine (**4**) (70.90%), 1,4-(diquinazolin-4-imine)benzene (**5**) (43.70%) and 2-(*p*-chlorophenyl)quinazolin-4-imine (**6**) (35.81%).

The compounds synthesized were characterized and the bioactivity of anti-oxidant of each compounds were tested by using DPPH radicals scavenging method. From the bioassay, all the 4*H*-3,1-benzoxazin-4-one derivatives compounds do not shows antioxidant as there is no free active hydrogen to stabilize the radical of DPPH. While all the quinazolin-4-imine derivative compounds synthesized shows good antioxidant ability as the IC_{50} is lower compare to ascorbic acid except for compound (**5**). Among the quinazolin-4-imine derivatives, 2-phenylquinazolin-4-imine shows the lowest IC_{50} value at 2.66ppm while the highest IC_{50} value belongs to 1,4-(diquinazolin-4-imine)benzene (**5**), which is 25.40ppm. From the IC_{50} values it can conclude that the present of electron withdrawing group at the phenyl substituent causes inductive effect to quinazolin-4-imine compounds and decreases its ability to donate hydrogen for antioxidant purpose.

REFERENCES

1. Saini, M. S., Kumar, A., Dwivedi, J., & Singh, R. (2013). A Review: Biological Significances of Heterocyclic Compounds. *International Journal of Pharma Science and Research*, **4**, 66-77.
2. Kumar, B. V., Vaidya, S. D., Kumar, R. V., Bhirud, S. B., & Mane, R. B. (2006). Synthesis and Anti-Bacterial Activity of Some Novel 2-(6-Fluorochroman-2-Yl)-1-Alkyl/Acyl/Aroyl-1h-Benzimidazoles. *Eur J Med Chem*, **41**(5), 599-604.
3. Chen, C. J., Song, B. A., Yang, S., Xu, G. F., Bhadury, P. S., Jin, L. H., Hu, D. Y., Li, Q. Z., Liu, F., Xue, W., Lu, P., & Chen, Z. (2007). Synthesis and Antifungal Activities of 5-(3,4,5-Trimethoxyphenyl)-2-Sulfonyl-1,3,4-Thiadiazole and 5-(3,4,5-Trimethoxyphenyl)-2-Sulfonyl-1,3,4-Oxadiazole Derivatives. *Bioorg Med Chem*, **15**(12), 3981-3989.
4. Palaska, E., Sahin, G., Kelicen, P., Durlu, N. T., & Altinok, G. (2002). Synthesis and Anti-Inflammatory Activity of 1-Acylthiosemicarbazides, 1,3,4-Oxadiazoles, 1,3,4-Thiadiazoles and 1,2,4-Triazole-3-Thiones. *IIFarmaco*, **57**, 101-107.
5. Cheng, J. H., Hung, C. F., Yang, S. C., Wang, J. P., Won, S. J., & Lin, C. N. (2008). Synthesis and Cytotoxic, Anti-Inflammatory, and Anti-Oxidant Activities of 2',5'-Dialkoxyhalcones as Cancer Chemopreventive Agents. *Bioorg Med Chem*, **16**(15), 7270-7276.

6. Rajput, R., & Mishra, A. P. (2012). A Review on Biological Activity of Quinazolinones. *International Journal of Pharmacy and Pharmaceutical Science*, **4(2)**, 66-70.
7. Fomsgaard, I. S., Mortensen, A. G., & Carlsen, S. C. (2004). Microbial Transformation Products of Benzoxazolinone and Benzoxazinone Allelochemicals--a Review. *Chemosphere*, **54(8)**, 1025-1038.
8. Ambujakshan, K. R., Varghese, H. T., Mathew, S., Ganguli, S., Nanda, A. K., & Panicker, C. Y. (2008). Vibrational Spectroscopic Studies and Theoretical Calculations of 2-Phenyl-4H-3,1-Benzoxazin-4-One. *Oriental Journal of Chemistry*, **24(3)**, 865-874.
9. Vince, R., & Hua, M. (1990). Synthesis and Anti-Hiv Activity of Carbocyclic 2',3'-Didehydro-2',3'-Dideoxy-2,6-Disubstituted Purine Nucleosides. *Journal of Medicinal Chemistry*, **33**, 17-21.
10. Osbone, A. G., & Goolamali, Z. (2000). ¹H and ¹³C NMR Spectral Studies of Some 4H-3,1-Benzoxazin-4-Ones and Their 2-Acylaminobenzoic Acid Precursors. *Spectrochimica Acta Part A*, **56**, 1079-1100.
11. D., P., Lampman, G., Kriz, G., & Vyvyan, J. (2008). Introduction to Spectroscopy. 4th Ed. Canada: Cengage Learning. 135.
12. Alagarsamy, V., Salomon, V. R., Vanikavitha, G., Paluchamy, V., Chandran, M. R., Sujin, A. A., Thangathirupathy, A., Amuthalakshmi, S., & Revathi, R. (2002). Synthesis, Analgesic, Anti-Inflammatory and Antibacterial Activities of Some Novel 2-Phenyl-3-Substituted Quinazolin-4(3H) Ones. *Biological & Pharmaceutical Bulletin*, **25(11)**, 1432-1435.

DEMETALLIZATION OF TOXIC AND HEAVY METALS IN CLAM, *PAPHIA TEXTILE* UTILIZING CATALYTIC CHELATION TECHNIQUE

Nur Syafiqah Mohamad Sa'adan , Wan Azelee Wan Abu Bakar, Wan Nur Aini Wan Mokhtar
Department of Chemistry, Faculty of Science, Universiti Teknologi Malaysia, 81310 Johor Bahru

Abstract

This research was carried out to study the toxic and heavy metals removal like lead (Pb), cadmium (Cd) and nickel (Ni) from *Paphia textile*. Three types of chelating agents, namely trisodium citrate, sodium acetate and disodium oxalate and three types catalysts supported on Al_2O_3 namely MgO, CaO and BaO were used. The demetallization treatment screening carried out at a 400 mg/L, one hour treatment time and treatment temperature of $32.5 \pm 0.5^\circ C$ on *Paphia textile*, revealed trisodium citrate was the most potential chelating agent. Metals concentration were analysed using Flame atomic absorption spectroscopy (FAAS). The initial concentration of Pb, Ni and Cd in *Paphia textile* were found to be $1.05 \pm 0.18 \mu g/g$, $0.83 \pm 0.21 \mu g/g$ and $0.56 \pm 0.02 \mu g/g$ respectively. The results on the optimization chelation technique showed that 400 mg/L of trisodium citrate gave the highest percentage removal of toxic and heavy metals with Pb 84.69% ($0.16 \pm 0.05 \mu g/g$), Ni with 78.60% ($0.18 \pm 0.08 \mu g/g$) and Cd with 41.96% ($0.33 \pm 0.01 \mu g/g$). Among the three catalysts studied, CaO/ Al_2O_3 catalysts at an optimum calcination temperature of $1000^\circ C$, in the presence of trisodium citrate, gave the highest percentage removal with 87.79% ($0.13 \pm 0.15 \mu g/g$) of Pb, 83.56% ($0.14 \pm 0.11 \mu g/g$) of Ni and 76.43% ($0.13 \pm 0.01 \mu g/g$) of Cd. This study showed that catalytic chelation technique at optimum conditions able to remove further the toxic and heavy metals compared to chelation technique from *P. textile* to achieve permissible limits set by Malaysian Food Regulation (Cd and Ni: $1.00 \mu g/g$; Pb: $2.00 \mu g/g$) and EU Regulation (Cd and Ni: $1.00 \mu g/g$; Pb: $1.50 \mu g/g$).

Keywords: Toxic and heavy metal, *Paphia textile*, Chelating agent, Catalyst, Flame Atomic Absorption Spectroscopy (FAAS)

INTRODUCTION

Paphia textile (Family: Veneridae) is known as Lala in Malaysia. *P. textile* is an infaunal filter-feeding which feed on phytoplankton, small zooplankton and other organic materials. This bivalve commonly found in the sandy-muddy bottoms of the internal and sublittoral zones of the coastal environment [1]. Basically, *P. textile* was found in Pantai Bagan Panchor until Pantai Remis, Perak of Peninsular Malaysia.

Heavy metals such as cadmium and mercury and toxic metals such as arsenic, lead, magnesium, manganese, selenium, vanadium, and essential metals such as copper and zinc could be classified as potentially dangerous heavy metals [2]. These heavy metals contribute to degradation of marine ecosystems by reducing species diversity and abundance and through accumulation of metals in living organisms and food chains [3]. The factors which influence metal concentration and accumulation are bioavailability of metals, season, size, sex, hydrodynamics of the environment, changes in tissue composition and reproductive cycle [4]. Basically, clams focused on the use of total soft tissues of clams rather than the clams shell as a quantitative indicator to reflect the heavy metal contamination in the coastal area. Basically, types of toxic and heavy metals found in clams are Cd, Cr, Cu, Fe, Pd, Ni, Hg and Zn and Fe is the highest concentration accumulated in the soft tissue of clams [5]. Concentration of heavy metals in clams revealed that Fe gives the high concentration by having 289 ppm [6]. One of the effective ways to treat heavy metals poisoning is through chelating technique [7]. Chelation technique is recommended for heavy metal poisoning and these metals exert their toxic substances by combining with one or more reactive groups essential for normal physiological functions. The chelating agent is the formation of ring-like structure that called as 'chelate' and the chelating agent will be bind to the metal ion and form a complexes before excrete out from the flesh. The used of catalysts is needed in order to enhance the chelation technique. The purpose of the study is to remove toxic and heavy metals (Pb, Ni and Cd) from contaminated *P. textile* using several types of chelating agents with addition of catalysts. The result should compliment with the permissible limit set by the Malaysian Food Regulations (1985) and Commission Regulation of EU (2006).

MATERIALS AND METHODS

Pb, Ni and Cd metals were analyzed through Flame atomic absorption spectroscopy, FAAS (Perkin Elmer Pin AAcle). All reagents used in the study were analytical grade and were used without any purification. All the solutions were prepared using distilled water. Samples were digested using HNO_3 (QRc™, 65%). All the plastic and glassware were cleaned by soaking in diluted HNO_3 and rinsed with distilled water. The element standard solutions used for calibration were produced by diluting a stock solution. The chelating agents used were sodium citrate dehydrate, $C_6H_5Na_3O_7 \cdot 2H_2O$ (QRc™), disodium oxalate, $Na_2C_2O_4$ (Bendosen) and

sodium acetate trihydrate, $\text{CH}_3\text{COONa} \cdot 3\text{H}_2\text{O}$ (QR $\text{\textcircled{C}}$ ™). Meanwhile for the catalyst, the chemicals were magnesium acetate tetrahydrate, $\text{C}_4\text{H}_6\text{O}_2\text{Mg} \cdot 4\text{H}_2\text{O}$ (Rinting Scientific), barium nitrate, $\text{Ba}(\text{NO}_3)_2$ (Sigma Aldrich) and calcium nitrate tetrahydrate, $\text{Ca}(\text{NO}_3)_2 \cdot 4\text{H}_2\text{O}$ (Sigma Aldrich). For standard solution for calibration, Pb, Ni and Cd pure single-element standards (Perkin Elmer) were used.

Catalyst Preparation

The catalyst was prepared by dissolving 6.25 gram of magnesium acetate tetrahydrate salt powder into 5 mL of distilled water and stir until the powder was dissolved. Alumina pallets were immersed into the solution. Later, it was aged at 80°C for 24 hours before further calcined at 1000°C for another 5 hours. Similar procedure was repeated to prepare 5 mol calcium nitrate tetrahydrate powder (5 gram in 5 mL distilled water) and 0.5 mol of barium nitrate powder (5 gram in 50 mL distilled water). All analysis was conducted in three series of replicates.

Sampling

Paphia textile was purchased from the wet market in Pasar Taman Universiti, Skudai. These clam samples were then brought back to laboratory and were stored in refrigerator until treatment.

Toxic and Heavy Metals Removal

Treatment for toxic and heavy metals removal in *P. textile* was conducted using three types of chelating agents. *P. textiles* were put in sack and were soaked in the beaker that contains the chelating agents with stirring for 1 hour. *P. textile* was rinsed with distilled water and digested before analyzed using FAAS. Chelation process was optimized using chelating agent (300 to 600 $\mu\text{L/L}$), for 1, 3 and 5 hours of treatment time and at different treatment temperature ($29.5 \pm 0.5^\circ\text{C}$, $32.5 \pm 0.5^\circ\text{C}$ and $37.5 \pm 0.5^\circ\text{C}$). For catalytic chelation treatment, samples were soaked in chelating solutions by immersing 0.25 g of prepared catalysts which put in sack in the solution and left it at the bottom of the solution.

Toxic and Heavy Metal Analysis

All prepared samples were digested using 65% of HNO_3 . The digestion was done until clear solutions were obtained. After the digestion process, the samples were allowed to cool and filtered using Whatman No 42 filter paper and then diluted to 10 mL with distilled water. The prepared samples were then analysed for Pb, Ni and Cd using FAAS. The concentrations are presented in $\mu\text{g/g}$. The standard solution and blank were also run for calibration.

RESULTS AND DISCUSSION

Toxic and Heavy Metal Concentration in *Paphia textile*

The initial concentrations of toxic and heavy metals in *P. textile* are presented in **Table 1**. The trisodium citrate was varied from 300 to 600 mg/L to get the optimum concentration of chelating agent. The obtained results from FAAS showed that the initial *P. textile* samples contain Pb a bit higher than permissible limit stated by European Union (EU) meanwhile, Cd and Ni concentration below the permissible limit stated by Malaysian Food Regulation (MFR) and European Union (EU) as stated in **Table 1**.

Table 1: Initial concentration of toxic and heavy metals in *P. textile* and the permissible limit of MFR and EU

	Cd ($\mu\text{g/g}$)	Ni ($\mu\text{g/g}$)	Pb ($\mu\text{g/g}$)
Initial Concentration	0.85 \pm 0.002	0.82 \pm 0.07	1.77 \pm 0.09
Permissible Limit:			
Malaysia	1.00	1.00	2.00
EU	1.00	1.00	1.50

The results of the three different chelating agents are presented in **Fig. 1**. The results indicated that trisodium citrate was the most effective chelating agents with the percentage removal of toxic and heavy metals (Pb: 84.69%, Ni: 78.60%, Cd: 41.96%) were obtained. The trisodium citrate gave the highest percentage removal of heavy metals in *P. textile* followed by sodium acetate and disodium oxalate. This trend showed that the high stability of the ring structured metal-citrate complex produced from chelation, thus increase the removal percentage of heavy metal ions [9].

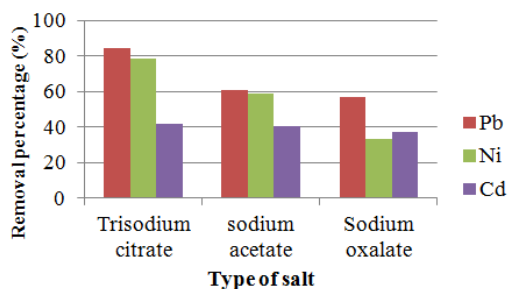


Fig. 1: Effect of chelating agent on toxic and heavy metals removal in *P. textile* at 400 mg/L trisodium citrate at 32.5±0.50°C for 1 hour.

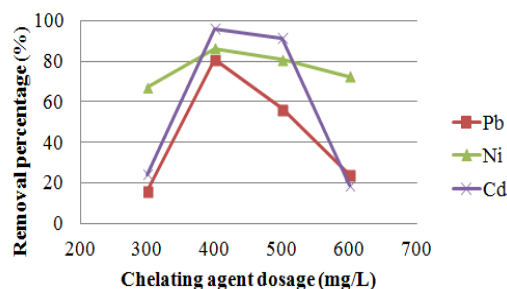
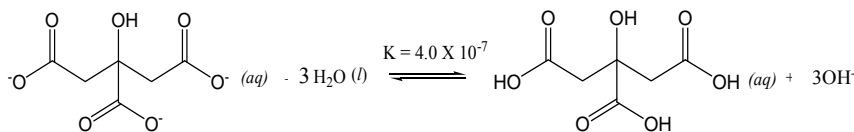


Fig. 2: Efficiency of trisodium citrate at different concentrations towards removal of toxic and heavy metals from *P. textile* at ambient temperature for 1 hour.

Optimization of Chelating Agents

The optimization treatment condition of chelation treatment by using trisodium citrate were at 400 mg/L concentration dosing, 32.5±0.50°C of treatment temperature and 5 hours treatment were initially selected as it gave the highest percentage removal of toxic and heavy metals in *P. textile*. Since one hour treatment was more practically used in laboratory and consumer's application thus, 1 hour of treatment time was applied for *P. textile* treatment with other chelating agents which are sodium acetate and disodium oxalate.

The efficiency of trisodium citrate at different concentrations in the removal of toxic and heavy metals concentration in *P. textile* is presented in **Fig. 2**. From the results it is revealed that the levels of toxic and heavy metals studied were successfully reduced by trisodium citrate treatment (Pb; 80.96%, Ni: 86.99% and Cd: 96.20%) and the concentration of 400 mg/L was found to be the most effective with highest percentage removal of toxic and heavy metals. The analysis suggests that there is a trend on toxic and heavy metals removal by trisodium citrate as the increased in dosing of chelating agents. The removal of the toxic and heavy metals increased and reached optimum at concentration of 400 mg/L. Exceeding this concentration, the percentage removal of toxic and heavy metals decreased accordingly. This pattern could be explained by Le Chatelier's principle [8] whereby the increased in concentration of trisodium citrate will enhance the reversible reaction towards the formation of starting material, thus decrease the citrate ion production to chelate the toxic and heavy metals.



Further investigating was done in the treatment time with varied to one, three and five hours. Results showed that the percentage removal of toxic and heavy metals removal increased as the time increased (**Fig. 3**). Five hours treatment showed the highest percentage removal of toxic and heavy metals (Pb: 71.65%, Ni: 57.36%, Cd: 50.70%). It is most probably the longer period of treatment time allowing the trisodium citrate to remove the toxic and heavy metals from *P. textile*.

Effect of temperature on the efficiency of trisodium citrate was studied and results are presented in **Fig. 4**. From the results, the percentage removal of toxic and heavy metals increased from 29.50±0.50°C to 32.50±0.50°C and decreased at 37.50±0.50°C. Highest percentage removal of toxic and heavy metals (Pb: 84.69%, Ni: 78.60%, Cd: 41.96%) was observed at 32.50±0.50°C. The increased with temperature up to

32.50±0.50°C may due to habitat of clams which can survive at 31.11°C thus, increase the mucus gland in clam and the percentage removal of toxic and heavy metals increased. On the other hand, toxic and heavy metals removal decreased at 37.50±0.50°C due to the high mucus gland from *P. textile* which covered the flesh surface and prevent the chelating agent to remove toxic and heavy metals.

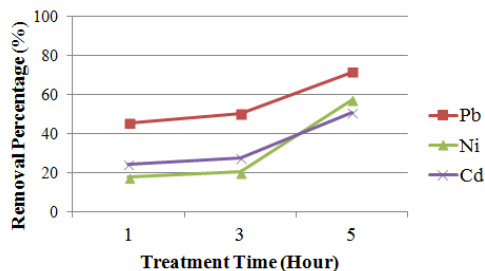


Fig. 3: Effect of treatment time on toxic and heavy metals removal in *P. textile* using 400 mg/L trisodium citrate at ambient temperature.

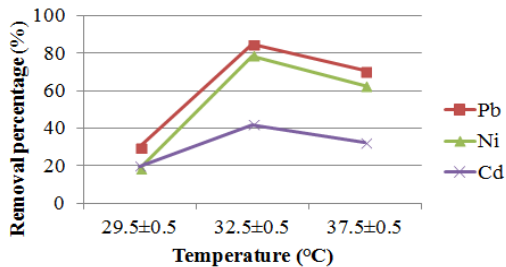


Fig. 4: Effect of reaction temperature on toxic and heavy metals removal in *P. textile* using 400 mg/L trisodium citrate for 1 hour.

Catalytic Activity

The study on the catalytic treatments was done to identify the effect of CaO, BaO and MgO supported with Al₂O₃ catalyst with 1000°C calcination temperature towards metals chelation of trisodium citrate. The heavy metals concentration with and without the presence of catalyst was determined. The results are presented in **Table 2**. The result showed that CaO/Al₂O₃ gave the highest percentage removal of toxic and heavy metals in *P. textile*. It indicates, with the presence of CaO/Al₂O₃ catalyst, the percentage removal of toxic and heavy metals increased compared without catalyst. Hence, the catalyst was optimized to get the optimum catalytic treatment. The increase in removal percentage of toxic and heavy metals probably due to the enhancement the formation of irreversible reaction by catalyst to produce the anion (citrate) which then reacts with the toxic and heavy metals in the contaminated *P. textile* [10].

The optimization for the treatment of catalyst, one hour treatment gives the highest percentage removal of toxic and heavy metals in *P. textile*. The results are presented in **Table 3**. The longer treatment duration with catalysts increased the frequency of catalytic chelation cycle and the possibility of the chelate ions to reach out the metal ions for complexation [10]. The removal percentages of heavy metals were not much different between 30 minutes and 45 minutes. Thus, from the results, it can shown that chelation technique and catalytic chelation technique can remove toxic and heavy metals in *P. textile* especially the catalytic chelation technique which can removed further towards heavy metals by having the highest percentage removal of toxic and heavy metals.

Table 2: Percentage removal of toxic and heavy metals in *P. textile* at 1000°C calcination temperature in trisodium citrate (400 mg/L) for 1 hour.

Chelating agents		Pb (µg/g)	Ni (µg/g)	Cd (µg/g)
Initial Concentration		1.05±0.18	0.83±0.21	0.56±0.02
Without catalyst		0.16±0.05	0.18±0.08	0.33±0.01
		84.69%	78.60%	41.96%
Calcined at 1000°C	CaO/Al ₂ O ₃	0.13±0.15	0.14±0.11	0.13±0.01
		87.79%	83.56%	76.43%
	MgO/Al ₂ O ₃	0.29±0.08	0.26±0.05	0.32±0.02
		72.17%	68.65%	43.09%
	BaO/Al ₂ O ₃	0.54±0.01	0.25±0.19	0.33±0.03
		48.58%	69.59%	41.09%

Table 3: Percentage removal of toxic and heavy metals in *P. textile* at 1000°C calcination temperature in trisodium citrate (400 mg/L) at different treatment times.

Chelating agents	Pb (µg/g)	Ni (µg/g)	Cd (µg/g)
Initial Concentration	1.05±0.18	0.83±0.21	0.56±0.02
Treated for 1 hour	0.13±0.15 87.79%	0.13±0.11 83.56%	0.13±0.01 76.43%
Treated for 45 min	0.47±0.11 55.15%	0.14±0.06 82.80%	0.30±0.00 46.39%
Treated for 30 min	0.46±0.08 56.34%	0.15±0.01 82.05%	0.31±0.02 44.90%
Treated for 15 min	0.52±0.010 50.95%	0.53±0.12 36.05%	0.27±0.04 52.03%

CONCLUSIONS

The chelation method is found to be a potential technique for the removal of toxic and heavy metals in *P. textile*. The optimization treatment conditions were obtained by having 400 mg/L trisodium citrate, one hour of treatment time and 32.50±0.50°C of treatment temperature. Present investigation illustrates the efficiency of the studied chelation agents in the order of trisodium citrate > sodium acetate > sodium oxalate. The trisodium citrate gave the highest percentage removal of toxic and heavy metals, whereby 84.69% (0.16±0.05 µg/g) of Pb, 78.60% (0.18±0.08 µg/g) of Ni and 41.96% (0.33±0.01 µg/g) of Cd. The highest percentage removal of toxic and heavy metals for catalytic chelation technique were achieved in the presence of CaO/Al₂O₃ catalysts, namely 87.79% (0.13±0.15 µg/g) of Pb, 83.56% (0.14±0.11 µg/g) of Ni and 76.43% (0.13±0.01 µg/g) of Cd at calcinations temperature 1000°C. In conclusion, both chelation and catalytic chelation technique can remove toxic and heavy metals. However, the catalytic chelation technique offers better removal of toxic and heavy metals from *P. textile* to achieve permissible limits set by Malaysian Food Regulation and EU Regulation.

REFERENCES

- Argente, F. A., Estacion, J. S., (2014). Effect of different harvesting practices on the dynamics of *Paphia textile* (Gmelin 1792) (Bivalvia: Veneridae) populations at two sites in Zamboanga del Norte, Southern Philippines. *Environmental and Experimental Biology* (12), 113-120.
- Al-Mohanna, S. Y., Subrahmanyam, M. N. V. (2001). Flux of heavy metal accumulation in various organs of the intertidal marine blue crab, *Portunus pelagicus* (L.) from the Kuwait coast after the Gulf War. *Environment International*, 27(4), 321-326.
- Hosono, T., Su, C., Delinom, R., Umezawa, Y., Toyota, T., Kaneko, S., Taniguchi, M., (2011). Decline in heavy metal contamination in marine sediments in Jakarta Bay, Indonesia due to increasing environmental regulations. *Estuar. Coast. Shelf Sci.* (92), 297-306.
- Krishna, Kumari, L., Kaisary, S., and Rodrigues, V. (2006). Bio-accumulation of some trace metals in the short-neck clam *Paphia malabarica* from Mandovi estuary, Goa. *Environment International*, 32(2), 229-234.
- Baby, J., Raj., J. S., Biby. (2010). Toxic effect of heavy metals on aquatic environment. *Int. J. Biol. Chem. Sci.* 4(4), 939-952.
- Juncharoenwongsa, N., Siriprom, W., Kaekhao, J., Chaeysuppaker, A., Limsuwan, P., Phachana, K., (2011). A Biomarkers Study: Trace Metal Elements in *Paphia Undulate* Shell for Assessing Pollution of Coastal Area. *Procedia Engineering* (8), 80-84.
- Sivakumar, S., Khatiwada, C. P., & Sivasubramanian, J. (2012). Bioaccumulations of aluminum and the effects of chelating agents on different organs of *Cirrhinus mrigala*. *Environmental Toxicology and Pharmacology*, 34(3), 791-800.
- Ihsan, W.A. (2013). *Catalytic Chelation Technique for the Removal of Toxic and Heavy Metals from Green Mussel, Perna viridis*. Master's thesis, Universiti Teknologi Malaysia, Skudai.
- Nurul Hazirah, M. (2013). *Removal of Toxic and Heavy Metals from Anadara granosa Using Chelating Agent*. Master's thesis, Universiti Teknologi Malaysia, Skudai.
- Hui, K.P. (2015). *Detoxification of Heavy Metals in Freshwater Catfish, Clarias spp. Utilizing Chelation and Catalytic Chelation Techniques*. Master's thesis, Universiti Teknologi Malaysia, Skudai.

DETERMINATION OF CHEMICAL COMPONENTS IN THE RHIZOMES OF *Hedychium coronarium*

Siti Nazeerah Binti Kamarruddin and Hasnah Binti MohdSirat

Department of Chemistry, Faculty of Science, Universiti Teknologi Malaysia, 81310 Johor Bahru.

Abstract

Hedychium coronarium locally known as white ginger lily belongs to Zingiberaceae family. Hydrodistillation of the fresh rhizomes yielded 0.02% of the essential oil. The composition of the essential oil was analyzed both by gas chromatography and gas chromatography-mass spectrometry. Eleven compounds were identified representing 79.78% of the whole compositions. 1,8-Cineole (39.03%) is the major component in the essential oil. Soxhlet extraction of the dried rhizomes of *H. coronarium* with chloroform as solvent yielded a crude extract 4.42%. Purification of the extract took place using column chromatography and preparative thin layer chromatography had afforded two diterpenes. Their structures have been identified using spectroscopic methods as two isomers of coronarin D (1.02%) and 14,15-dihydroxy-labda-8(17),12-diene-15,16-olide (coronarin G) (0.1%). Antioxidant property was screened using DPPH radical scavenging assay and has been carried out on the chloroform crude extract, essential oil and two pure compounds. The results revealed that the crude extract gave moderate antioxidant property with IC_{50} 275.05 μ g/mL. The antibacterial assay was conducted on chloroform crude extract, essential oil and coronarin D. Coronarin D was found to show moderate antibacterial property towards Gram positive bacteria *Bacillus subtilis* (BS) ATCC 6633 at a concentration of 450 ppm.

Keywords: *Hedychium coronarium*, labdane, coronarin, essential oil, bioassay.

INTRODUCTION

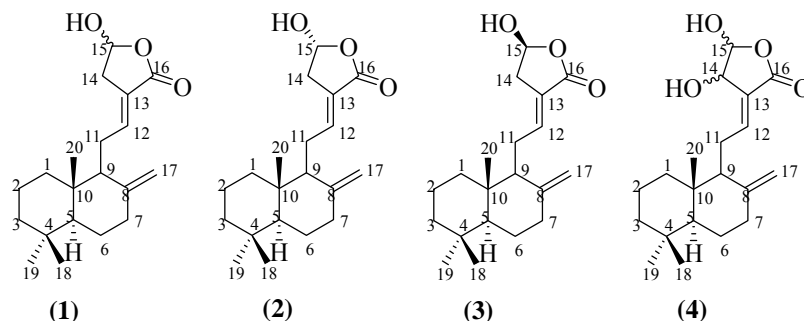
H. coronarium which has many common names including butterfly ginger, butterfly lily, cinnamon jasmine, garland flower, and ginger lily, is widely cultivated in India, Southeast Asian countries, South China, Taiwan, Japan, and Brazil. The rhizomes of *H. coronarium* is used in Chinese natural medicine, which has been prescribed for the treatment of headache, lancinating pain, contusion inflammatory, and sharp pain due to rheumatism in Chinese traditional preparations, while it is used as a febrifuge, tonic, excitant, and anti-rheumatic in the Ayurvedic system of traditional Indian medicine [1].

The chemical composition of the essential oils of ginger lily have been identified in the early studies such as α -muurolol (16.8%), α -terpineol (15.9%), 1,8-cineole (11.2%), α -fenchyl acetate (5.6%), citronellal (5.5%) and (*E*)-methyl cinnamate (5.1%). Some of the compounds that are present in the rhizomes of *H. coronarium* are the labdane diterpenes, (*E*)-labda-8(17),12-diene-15,16-dial, coronarin B, coronarin D, isocoronarin D, labda-8(17),11,13-trien-15,16-olide, an ester of labda-8(17),11,13-trien-15-al-16-oic acid and isocoronarin D, and 7 β -hydroxycoronarin B [2]. This research focused on the study of the rhizomes of *H. coronarium* and the objectives of this study are to extract the essential oil, phytochemical and to evaluate the bioactivity of *H. coronarium*. Purification of the chemical constituents present in the crude extracts of the rhizomes of *H. coronarium* and also to elucidate the structure of the compound using spectroscopic methods.

EXPERIMENTAL

Chemical composition analysis of the essential oil was carried out using a Gas Chromatography (GC) Hewlett Packard 5890 series II. A GC equipped with an Ultra 1 column (25 m long, 0.32 μ m thickness and 0.17 mm internal diameter). The chromatogram of gas chromatography-mass spectrometry (GC-MS) was recorded using a Perkin Elmer Gas Chromatograph Clarus 680 equipped with mass Spectrometer Clarus SQ 8 S. All chemicals involved in this experiment are analytical grade. Soxhlet extraction, fractionation and purification were carried out using several types of organic solvents which are *n*-hexane, petroleum ether, diethyl ether, chloroform, methanol and ethyl acetate. Petroleum ether refers to PE with a boiling point 60-80°C and was redistilled before used. Thin layer chromatography (TLC) was carried out on 0.20 mm Merck silica gel plates (60 F254). Samples were spotted on the baseline (0.5 cm) drawn on the TLC. The compounds were visualized under a UV lamp (254 nm) and vanillin sulphuric acid spray. Fractionation and purification of the crude extracts were conducted using gravity column chromatography (CC) and preparative thin layer chromatography (prep TLC) with Merck silica gel 70-230 mesh and silica gel 60 PF254 (10-40 μ) containing gypsum, respectively. Infrared (IR) spectra were recorded on Perkin Elmer 1650 FTIR spectrophotometer using the attenuated total reflection (ATR) for the gummy samples. The ¹H and ¹³C nuclear magnetic resonance spectra (NMR) were recorded on Bruker Avance 400 Spectrometer (400 MHz and 100 MHz respectively). Deuterated chloroform was used as solvent.

Intensity of the colour change of DPPH for antioxidant assay were recorded on Biotek Epoch Microplate Spectrophotometer. The wavelength was set to 517nm.



Plant Material

The sample of *H. coronarium* or also known as ginger lily was obtained from Skudai, Johor in 2014.

Extraction and Isolation

The fresh chopped rhizomes (205.0 g) were extracted using hydrodistillation technique in a Dean-Stark apparatus for 8 hours. The essential oil collected was extracted with ether (3×10 mL), dried over anhydrous magnesium sulphate and filtered. The ether was then evaporated at room temperature overnight to give the essential oil (0.039 g, 0.02%) as pale yellow oil with a fragrant scent.

The rhizomes of *H. coronarium* (74.0 g) were air dried, powdered and extracted with chloroform in a Soxhlet apparatus for 20 h. The resulting chloroform extract was evaporated to dryness under reduced pressure using rotary evaporator to afford a thick dark yellowish brown gum crude extract labeled as HC (3.3 g, 4.5%). The crude extract HC (2.0 g) obtained was purified using column chromatography (CC) (100×3.5 cm length) packed with Merck silica gel 70-230 mesh (60 g). The column was eluted using n-hexane and Et₂O as solvent with increasing polarity gives eight major compounds. Fraction HC 5 was evaporated under reduced pressure to give a mixture of epimers of coronarin D (**1**) (0.0203 g, 1.02%) as a dark yellowish brown gum. Further purification of fraction HC 4 using prep TLC afforded another four compounds using triple development with n-hexane and Et₂O (2:1). Fraction HC 4-4 was concentrated to give a compound that was tentatively predicted as 14,15-dihydroxyabda-8(17),12-diene-15,16-olide (Coronarin G) (**4**).

RESULTS AND DISCUSSION

The essential oil of *H. coronarium* was analysed by GC and GC-MS. The mass spectrum of each peak was compared with mass spectrum from the National Institute of Standards and Technology (NIST). The high percentage matching (more than 80%) was selected as the constituents. The identified constituents of the essential oil of *H. coronarium* are listed in **Table 1**. A total of eleven components were successfully identified from the GC and GC-MS comprising 79.78% of the total. The essential oil consisted of only monoterpenes with 1,8-cineole (39.03%) as the main constituent. The other major components found in the rhizome oil were α -terpineol (21.67%) and β -pinene (8.05%). Previous study showed that the major essential oil components of *H. coronarium* from Mauritius is α -muurolol (16.8%), α -terpineol (15.9%), 1,8-cineole (11.2%), α -fenchyl acetate (5.6%), citronellal (5.5%) and (*E*)-methyl cinnamate (5.1%) [3]. Meanwhile another research from India reported that the major constituents of fresh rhizome oil were 1,8-cineole (41.42%), β -pinene (10.39%), α -terpineol (8.80%) and α -pinene (4.06%) [4]. The chemical composition of rhizome oil of *H. coronarium* collected in Johor, Malaysia was closely resemble to the essential oil composition reported by Beena Joy [4], in which 1,8-Cineole is the major component.

Coronarin D epimers (**1**) were obtained as dark yellowish brown gum (0.02 g, 1.02 %) with a R_f 0.38 (n-hexane:Et₂O, 1:2). The IR spectrum showed that there is weak hydroxyl bend at the position of 3373 cm⁻¹. The spectrum also showed a sharp bend at 1737 cm⁻¹ for carbonyl C=O ester in the furan ring. It could be observed that the bend is shifted to a lower value due to the conjugation of double bond outside the ring causing it to weakened the strain of C=O bond. The ¹H NMR spectrum of compound (**1**) revealed the presence of a mixture of coronarin D epimers (**2**) and (**3**). The proton NMR spectrum showed three singlet integrating for three proton

each at δ 0.72, δ 0.82 and δ 0.89 which were attributed to three methyl groups. Two broad singlet proton resonated at δ 4.40 and δ 4.82 was assigned to exomethylene protons at C-17. These suggested that compound (1) has a labdane type skeleton. The epimers are assigned as coronarin D (A) (2) and coronarin D (B) (3). The position of the first set exomethylene could be given to compound (2), meanwhile for compound (3) two weak doublet protons resonated at δ 4.35 and δ 4.82 with a value of proton coupling $J = 0.8$ Hz. As for the ^1H - ^1H COSY spectrum for compound (1) showed the correlation between H-11, H-14 and H-17. The ^{13}C NMR supported the presences of 23 peaks with three extra peaks due to the epimeric mixture that contains in compound (1). The duplicate peaks were at the position of C-8, C-12 and C-17 which can be assigned to one set to compound (2) while the other set belongs to compound (3). Analysis of DEPT spectrum showed the existing of three methyl group at δ 33.58 (C-18), δ 21.73 (C-19) and δ 14.35 (C-20); one exomethylene at δ 107.36 (C-17) for compound (2) while the other at δ 107.65 (C-17) for compound (3) and seven methylene at δ 39.21 (C-1), δ 19.32 (C-2), δ 41.99 (C-3), δ 24.09 (C-6), δ 37.78 (C-7), δ 25.51 (C-11) and δ 124.48 (C-14); and four methine groups at δ 55.33 (C-5), δ 56.12 (C-9), δ 96.46 (C-15) and δ 143.55 (C-12) for compound (2) while the other at δ 143.64 (C-12) for compound (3). The complete assignments of the carbons were accomplished by the HMQC spectrum. The complete ^1H NMR and ^{13}C NMR parameters for coronarin D (1) epimers are listed in Table 2.

Table 1: Chemical composition of the essential oil of *H. coronarium*

No.	Compounds	Kovats Index	Percentage of Composition (%)
1	α -Pinene	928	1.81
2	β -Pinene	964	8.05
3	Myrcene	980	2.77
4	α -Phellandrene	997	0.47
5	1,8-Cineole	1017	39.03
6	<i>E</i> -Sabinene hydrate	1055	0.89
7	Linalool	1094	1.49
8	Camphor	1117	0.31
9	Pinocarvone	1132	0.90
10	Terpinen-4-ol	1160	2.39
11	α -Terpineol	1171	21.67
Total amount identified (%)			79.78

Table 2: ^1H and ^{13}C NMR data of compound (1)

Carbon	^1H (δ ppm)	^{13}C (δ ppm)
1	1.00-2.10	39.21
2	1.00-2.10	19.32
3	1.00-2.10	41.99
4	-	33.58
5	1.00-2.10	55.33
6	1.00-2.10	24.09
7	2.30-2.40 m	37.78
8	-	147.91/148.12
9	1.00-2.10	56.12
10	-	39.44
11	2.20/2.35	25.51
12	6.73 m	143.55/143.64
13	-	124.48
14	2.73 dd $J = 2, 15.2/$ 3.00-3.06 m	33.56
15	5.95 m	96.46
16	-	170.66
17	4.35/4.82 d $J = 0.8$ Hz 4.40/4.82 s	107.36/107.65
18	0.89 s	33.58
19	0.82 s	21.73
20	0.72 s	14.35

Preparative TLC of HC4 using *n*-hexane:Et₂O (1:1) afforded a minor constituent HC4-4 as a pale yellow oil (2.0×10^{-3} g, 0.1 %) with R_f 0.5 (*n*-hexane:Et₂O, 1:1). The ¹H NMR spectrum HC4-4 revealed the presence of three singlet each integrating for three proton at δ 0.71, δ 0.82 and δ 0.89 and exomethylene proton at δ 4.57 and δ 4.89 suggested that HC4-4 has the labdane skeleton. Two deshielded protons were observed at δ 6.82 and δ 6.11 which were assign to be β -olefinic proton at C-12 and methine proton at C-14 respectively. Another broad singlet at δ 3.67 was an oxymethine proton at C-14. Due to insufficient amount of sample the compound (4), the ¹³C NMR was not obtained to support the structure of compound. Therefore tentatively the compound was assigned as 14,15-dihydroxyabda- 8(17),12-diene-15,16-olide (Coronararin G) (4).

Antioxidant activity was screened using DPPH radical scavenging assay and has been carried out on the chloroform crude extract, essential oil and two pure compounds. The results revealed that the crude extract gave moderate antioxidant property with IC₅₀ 275.05 μ g/mL. The antibacterial assay was conducted on chloroform crude extract, essential oil and coronarin D. Coronarin D was found to show moderate antibacterial properties towards Gram positive bacteria *Bacillus subtilis* (BS) ATCC 6633 at a concentration of 450 ppm.

CONCLUSION

The extraction of the fresh rhizomes by hydrodistillation afforded essential oil in 0.02% yielded. By GC and GC-MS analyzed revealed eleven compounds which contributed 79.78% of the total oil. Meanwhile, Soxhlet extraction of *H. coronarium* yielded chloroform extract (4.42%). Purification of chloroform extract have resulted in the isolation of two labdane diterpene compounds. The compounds were identified by using spectroscopic techniques and also by comparison with the literature value and the first compound has be proposed as epimers of coronarin D (34). As for the second compound, it was tentatively identified as 14,15-dihydroxyabda-8(17),12-diene-15,16-olide (coronararin G) (51). The DPPH free radical scavenging activity screening showed that the crude chloroform extract gave positive antioxidant, whereas epimer of coronarin D was active towards *Bacillus subtilis* (Gram positive bacteria).

REFERENCES

1. Matsuda, H., Morikawa, T., Sakamoto, Y., Toguchida, I., and Yoshikawa, M. (2002). Labdane-type Diterpenes with Inhibitory Effects on Increase in Vascular Permeability and Nitric Oxide Production from *Hedychium coronarium*. *Bioorganic & Medicinal Chemistry*, **10**(8), 2527-2534.
2. Nakatani, N., Kikuzaki, H., Yamaji, H., Yoshio, K., Kitora, C., Okada, K., and G. Padolina, W. (1994). Labdanediterpenes from rhizomes of *Hedychium coronarium*. *Phytochemistry*, **37**(5), 1383-1388.
3. Gurib-Fakim, A., Maudarbaccus, N., Leach, D., Doimo, L., and Wohlmuth, H. (2002). Essential Oil Composition of Zingiberaceae Species from Mauritius. *Journal of Essential Oil Research*, **14**(4), 271-273.
4. Joy, B., Rajan, A., and Abraham, E. (2007). Antimicrobial activity and chemical composition of essential oil from *Hedychium coronarium*. *Phytotherapy Research*, **21**(5), 439-443.

FERRITE-CALCIUM ALGINATE AS MAGNETIC SOLID PHASE EXTRACTION ADSORBENT OF COPPER(II) IONS IN WATER PRIOR TO FLAME ATOMIC ABSORPTION SPECTROSCOPY

Nur Syafika Shah Bani^a, Wan Aini Wan Ibrahim^{a*} and Hamid Rashidi Nodeh^a

^aDepartment of Chemistry, Faculty of Science, Universiti Teknologi Malaysia, 81310 UTM Johor Bahru, Johor, Malaysia

Abstract

A magnetic solid phase extraction (MSPE) procedure using ferrite-calcium alginate ($\text{Fe}_3\text{O}_4\text{-CaAlg}$) as adsorbent for Cu(II) ions prior to flame atomic absorption spectroscopy (FAAS) was developed. The extraction of Cu(II) ions using $\text{Fe}_3\text{O}_4\text{-CaAlg}$ MSPE is simpler and faster than the conventional method such as solid phase extraction and traditional method such as liquid-liquid extraction. The simple extraction is based on the use of magnetisable adsorbent to extract Cu(II) ions, which can be readily isolated from water samples as a matrix with an external magnet. The adsorbent was prepared by mixing sodium alginate solution with Fe_3O_4 magnetic particles and calcium chloride solution to form magnetic alginate beads. Important parameters influencing the extraction and desorption process including type and volume of desorption solvent, agitation time, extraction time, weight of adsorbent and ample volume were optimized. Under the optimized conditions, calibration graph (external standard method) with coefficient of determination (R^2) of 0.974 in the linearity range 20-100 $\mu\text{g/L}$ was observed. Good limit of detection (1.70 $\mu\text{g/L}$), and limit of quantification (5.6 $\mu\text{g/L}$) was obtained. Acceptable repeatability ($n = 3$) with RSDs 2.37% while reproducibility ($n = 9$) with RSD 5.15% were obtained for Cu(II) ions using the developed MSPE method. Finally, the proposed method was successfully applied for the determination of Cu(II) ion in tap water sample with relative recovery of 78.9% and 4.72% RSD. However, the proposed method was found to be less suitable for the determination of Cu(II) ion in river water sample with lower relative recovery (45.7% , 1.76% RSD) indicating that the method is sensitive to the matrix.

Keywords: Fe_3O_4 -Calcium alginate, Magnetic solid phase extraction, Copper(II) ions, Water samples, flame atomic absorption spectrophotometry

INTRODUCTION

Copper (Cu) are extensively used in industry field such as electroplating, manufacture of electrical wire and industrial machinery since it has good resistance to corrosion, low thermal expansion and tensile strength. As well as for industry uses, Cu also has been recognized as an essential trace metal for living organisms and important for human's growth and development. However, the amount of consumption has to be limit to 1–3 mg per day as an adequate and safe level of intake (Ndlovu et al., 2012) since it will affect human's health and causing several disease if excessive. According to Guidelines for Drinking-water quality of the World Health Organisation, the limit for copper content in drinking water is 2.0 mg/L (Jana et al., 2011). Above this healthy limit, copper will accumulate in the liver and become toxic to human which causing diarrhoea, vomiting and neurological illness such as schizophrenia, depression, autism and epilepsy (Shrivastava & Kumar, 2013). Since Cu has been widely used in industry and household plumbing, it will easily enter the environmental and water systems in a form of ion causing high exposure of people to Cu(II) ion residue by drinking water. Thus, method to remove Cu(II) ion from water supplies need to be developed to ensure the concentration is below the safety limit.

A simple, efficient and green sample preparation technique is required to replace conventional extraction techniques. In recent years, an alternative solvent minimization sample preparation approach, magnetic solid phase extraction (MSPE), has gained considerable attention. The advantages of the MSPE method are that this procedure is simpler and faster than LLE and SPE by the use of only an external magnetic force to isolate the adsorbent and analyte/s from sample matrix. Besides that, MSPE technique only requires small amount of organic solvent. With the advantages of MSPE, the development of modified Fe_3O_4 MNPs has to be developed and progress rapidly in order to improve the adsorption quality of the adsorbent and obtain the most efficient extraction results.

Alginates are natural anionic polysaccharide of brown algae which is composed of linear binary copolymers of (1-4)-linked β -D-mannuronic acid (M) and α -L-guluronic acid (G) monomers (Figure 1) (Draget et al., 2005). Due to high stiffness of gelling properties (Fuhrer & McHugh, 2003), high porosity and small size providing larger surface area (Paques et al., 2014), alginate has been applied as the adsorbent which encapsulate the Fe_3O_4 MNPs during the extraction of analyte. The polymer also consist of many carboxyl and hydroxyl groups which acts as potential adsorption sites for metal ions to bind (Draget et al., 2005).

In this study, a green MSPE analytical method was introduced by utilizing ferrite-calcium alginate ($\text{Fe}_3\text{O}_4\text{-Ca Alg}$) as the adsorbent. Calcium alginate (CaAlg) has the potential to be an effective adsorbent while MSPE is a simple and fast technique that contributes to minimize the time consuming, and use of organic solvent.

Thus, we consider this $\text{Fe}_3\text{O}_4\text{-CaAlg}$ MSPE approach as it is effective and gives higher relative recoveries of Cu(II) ion.

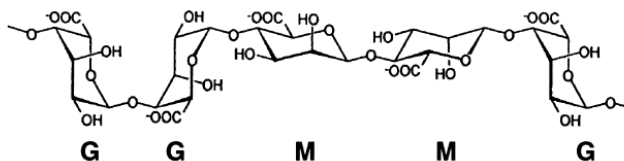


Figure 1: Chain conformation of (1-4)-linked β -D-mannuronic acid (M) and α -L-guluronic acid (G) polymer (Draget et al., 2005)

EXPERIMENTAL

Chemicals and Reagents

Water samples used were tap and river water from Sungai Skudai, Skudai, Johor. The glassware used in this project was washed with deionized water (DW) and have been sterilized. The $\text{Fe}_3\text{O}_4\text{-CaAlg}$ adsorbent was obtained (previously synthesised) from the analytical laboratory in Universiti Teknologi Malaysia, Johor. Deionized water was used all the time when preparing stock and standard solution. Cu stock solution (1000 mg/L) was prepared from CuSO_4 obtained from analytical laboratory in Universiti Teknologi Malaysia, Johor. Then, Cu standard solution of 1, 2, 3, 4, and 5 mg/L were prepared from the stock solution. The desorption solvents used were nitric acid (HNO_3), hydrochloric acid (HCl) and sulphuric acid (H_2SO_4). Nitric acid, 65% was purchased from QRec (Asia) Sdn Bhd (Selangor, Malaysia), hydrochloric acid 36.5-38.0% was purchased from J.T. Baker (Philipsburg, USA) and sulphuric acid 95-97% was obtained from Merck (Darmstadt, Germany). All desorption solvents namely 0.1 M of each of HNO_3 , HCl, H_2SO_4 and 1:1 mixture of HCl + HNO_3 were prepared by appropriate dilution of the concentrated solution.

Analytical Instrumentation

A PinA Aclé 900T FAAS equipped with deuterium background correction and a copper hollow cathode lamp was used for absorbance measurements at 324.75 nm. All measurements were carried out in an air/acetylene flame. Instrumental parameters used were those recommended by the manufacturer.

Preparation of stock, standard solutions and real water samples

The Cu stock solution (1000 mg/L) was prepared by dissolving 0.25 g of copper sulphate (CuSO_4) in DW. The solution was made up to the 100 mL mark in a volumetric flask. Then, a series of standard solutions (1.0, 2.0, 3.0, 4.0, 5.0) mg/L were prepared by appropriate dilution of the stock solution. River water sample and fresh tap water sample were collected in bottles pre-cleaned with acetone. For the river water samples, the samples were filtered through a Whatman filter paper No. 1 (Maidstone, England) to remove any non-soluble particles. The samples were stored in freezer at 5°C until analysis.

Preparation of $\text{Fe}_3\text{O}_4\text{-CaAlg}$ Adsorbent

An amount of 4.5 g of sodium alginate was accurately weighed and dissolved in 200 mL deionized water with magnetic stirring. A calcium chloride solution was prepared by mixing 33 g of the salt with 1.5 L of DW, with magnetic stirring. For encapsulation process to form $\text{Fe}_3\text{O}_4\text{-CaAlg}$ adsorbent, 4.0 g of the Fe_3O_4 MNPs were mixed with sodium alginate solution forming $\text{Fe}_3\text{O}_4\text{-NaAlg}$ solution. Then the $\text{Fe}_3\text{O}_4\text{-NaAlg}$ solution was slowly dropped into the calcium chloride solution. $\text{Fe}_3\text{O}_4\text{-CaAlg}$ beads were formed immediately in the calcium chloride solution. Lastly, the $\text{Fe}_3\text{O}_4\text{-CaAlg}$ beads were thoroughly rinsed with distilled and deionized water to eliminate any residues of calcium and chloride ions. $\text{Fe}_3\text{O}_4\text{-CaAlg}$ beads were placed in the oven for 12 h to dry the water residue.

$\text{Fe}_3\text{O}_4\text{-CaAlg}$ Magnetic Solid Phase Extraction Process and Optimization

The MSPE process is illustrated schematically in Figure 2. Briefly, 10 mL of water sample containing 1 mg/L of Cu(II) analyte from the prepared stock solution was added with 50 mg of $\text{Fe}_3\text{O}_4\text{-CaAlg}$ adsorbent. Initially,

the mixture was shaken for 30 min to allow adsorption process of Cu(II) ion onto the Fe₃O₄-CaAlg adsorbent. The adsorbent was then collected easily and quickly by applying an external magnet on the beaker wall, and the supernatant was decanted directly. For desorption of Cu(II) ion from the Fe₃O₄-CaAlg adsorbent, 3 mL of approximately 0.1 M solution of the desorption solvent was added into the beaker containing the adsorbent, and agitated for about 5 min. The adsorbent was then collected with an external magnet outside and the eluent was collected eluent for analysis using FAAS.

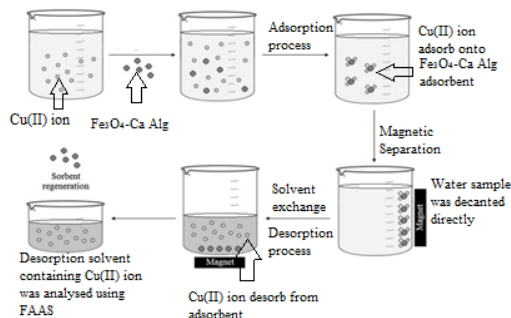


Figure 2: Schematic of Fe₃O₄-CaAlg MSPE process for Cu(II) ions from aqueous solution

In this study, three extraction and three desorption conditions were systematically optimized. Optimization of MSPE process was performed by varying one parameter at a time. The extraction parameters optimized were extraction time, weight of adsorbent and volume of sample while the desorption parameters optimized were types of desorption solvent, volume of desorption solvent and agitation time. Initially

RESULTS AND DISCUSSIONS

Effect of Desorption Solvent

In order to maximize the desorption of Cu(II) ion from Fe₃O₄-CaAlg adsorbent, a suitable solvent is required. Four different solvents namely 0.1 M HNO₃, 0.1 M HCl, 0.1 M H₂SO₄ and 0.1 M of a 1:1 mixture of HNO₃: HCl were used. During desorption of the Cu(II) ions, hydrogen ions were dissolved from the acid desorption solvent used and displaced the Cu(II) ions on the adsorbent. It was found that all the solvents examined showed almost equal desorption efficiency with recovery of Cu(II) ion in the range of 57.6%-61.6% but the highest percentage recovery was obtained with 1:1 mixture of HNO₃: HCl as the desorption solvent (Figure 3). Thus 1:1 mixture of HNO₃: HCl was selected for further analysis.

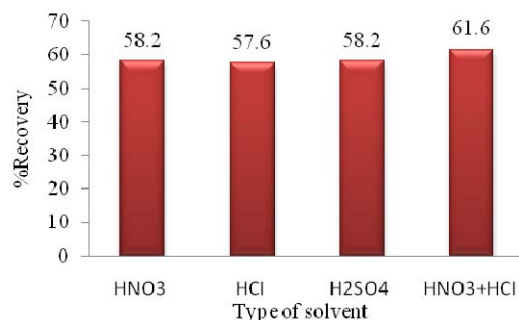


Figure 3: Effect of types of desorption solvent on Fe₃O₄-CaAlg MSPE of Cu(II) ion from water sample. Extraction conditions: 10 mL volume sample; 50 mg adsorbent weight; 30 min extraction time; Desorption conditions: 3 mL solvent volume with 5 min agitation time.

Effect of desorption solvent volume

In order to study the effect of desorption solvent on the recovery of Cu(II) ion, different volumes of the 1:1 HNO₃-HCl desorption solvent were optimized. This is to ensure quantitative recovery with minimum volume of

desorption solvent. Thus, the 0.1 M 1:1 mixture of HNO_3 +HCl solvent was set (3, 4 and 5 mL). Figure 4 shows that the percentage recovery of Cu(II) decreases as the desorption solvent increases from 3 to 5 mL. Desorption of Cu(II) ion from the Fe_3O_4 -CaAlg adsorbent was most effectively achieved using 3 mL of the optimized solvent. This indicates that 3 mL of the desorption solvent was sufficient to desorb adsorbed Cu(II) ions from the adsorbent. Thus, 3 mL of the 1:1 mixture of HNO_3 +HCl solvent was selected for further analysis.

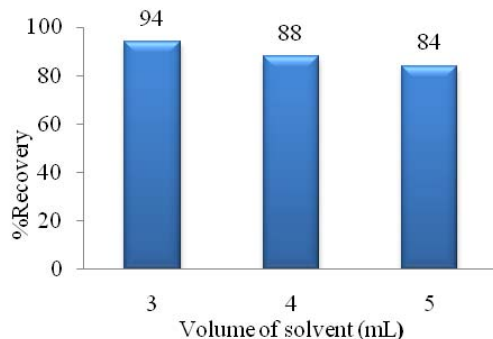


Figure 4: Effect of desorption solvent volume on Fe_3O_4 -CaAlg MSPE of Cu(II) ion from water sample. Extraction conditions: 10 mL volume of sample; 50 mg mass of adsorbent; 30 min extraction time; Desorption conditions: 1:1 mixture of HNO_3 +HCl desorption solvent with 5 min agitation time

Effect of extraction time

Generally, sufficient time is required to achieve adsorption equilibrium for the analyte on the adsorbent. In this study, the effect of extraction time on the extraction efficiency of Cu(II) ion on Fe_3O_4 -Ca Alg adsorbent was investigated by changing the extraction time from 1 to 60 min under the optimum conditions. Five sample solutions were continuously shaken using an orbital shaker at room temperature at 250 rpm. From the results obtained (Figure 5), it can be seen that equilibrium was reached within 5 min extraction time by showing recovery 104.5%. Decrease of percentage recovery was observed starting from 10 to 60 min extraction time. This might due to back-extraction of Cu(II) ion from Fe_3O_4 -CaAlg adsorbent into sample solution since ion exchange between cation group of adsorbent and Cu(II) ion in the water sample is reversible and the bond formed is just temporary (Wierucka & Biziuk, 2014). Thus, 5 min was selected for further analysis.

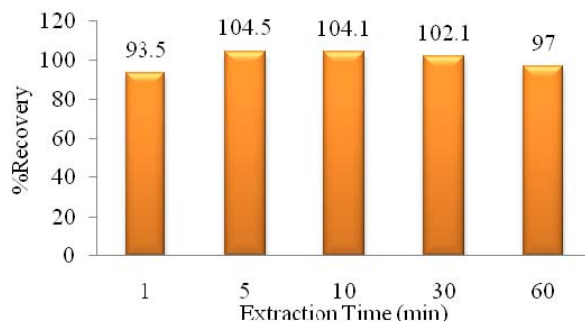


Figure 5: Effect of extraction time on Fe_3O_4 -CaAlg MSPE of Cu(II) ion from water sample. Extraction conditions: 10 mL volume of sample; 50 mg mass of adsorbent; Desorption conditions: 3 mL of 1:1 mixture of HNO_3 +HCl desorption solvent with 5 min agitation time

Effect of agitation time

In order to examine the influence of desorption time on the recovery of Cu(II) ions, different desorption time in the range of 30 to 300 s were optimized to ensure quantitative recovery of Cu(II) ions. The percentage recovery of Cu(II) ions increase as the desorption time increase from 30 s to 60 s but slightly decrease was observed at 120 s and 300 s. This might due to re-adsorbed of analyte by the adsorbent (Figure 6). Therefore, desorption time of 60 s was selected for further analysis for maximum desorption of analyte from adsorbent.

Effect of weight of adsorbent

Various weight (5 to 100 mg) of the $\text{Fe}_3\text{O}_4\text{-CaAlg}$ adsorbent were used to study its effect on adsorption of Cu(II) ions. Based on the results obtained (Figure 7), increase in weight of adsorbent increase the extraction efficiency probably due to more adsorption sites or surface area available for Cu(II) ions to be adsorbed. However, a further increase in the weight of adsorbent higher than 50 mg did not cause significant improvement in the adsorption of Cu(II) ions. This might due to the adsorption of Cu(II) ions onto the adsorbent was completed (Paques et al., 2014). Thus, higher weight of adsorbent was not necessary to reduce analysis cost. Thus, 50 mg adsorbent was used for further analysis.

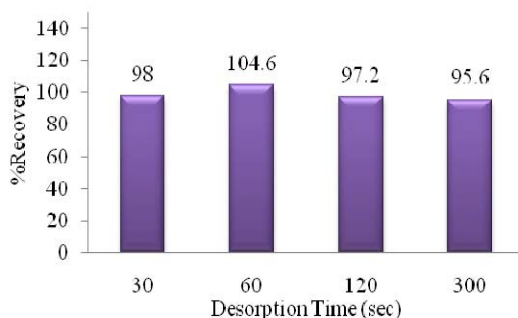


Figure 6: Effect of desorption time on $\text{Fe}_3\text{O}_4\text{-CaAlg}$ MSPE of Cu(II) ion from water sample. Extraction conditions: 10 mL volume of sample; 50 mg mass of adsorbent; 5 min extraction time; Desorption conditions: 3 mL of 1:1 mixture of $\text{HNO}_3\text{+HCl}$ desorption solvent

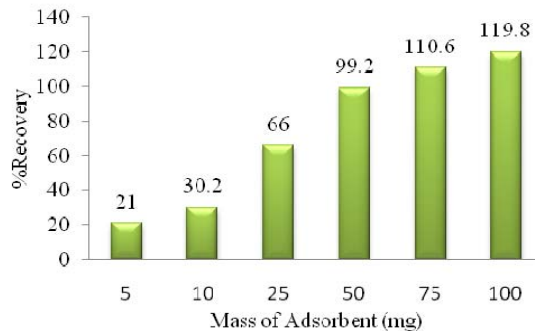


Figure 7: Effect of weight of $\text{Fe}_3\text{O}_4\text{-CaAlg}$ adsorbent on MSPE of Cu(II) ions from water sample. Extraction conditions: 10 mL sample volume; 5 min extraction time; Desorption conditions: 3 mL of 1:1 mixture of $\text{HNO}_3\text{+HCl}$ desorption solvent with 1 min agitation time

Effect of sample volume

In order to study the ability of the optimized weight of adsorbent in adsorbing Cu(II) ions different sample volumes were optimized. A series of 150 - 400 mL sample solutions containing 20 $\mu\text{g/L}$ of Cu(II) ions were prepared. Based on the results obtained, 50 mg of adsorbent was found to sufficient to adsorb the highest Cu(II) ions from 150 mL sample (Figure 8). Increase in the sample volume was found to decrease the % recovery. This might due to breakthrough volume of adsorbent which have been exceeded. Thus, 150 mL sample volume was selected for further analysis.

Method Validation

The $\text{Fe}_3\text{O}_4\text{-CaAlg}$ MSPE method was validated using the optimized conditions (50 mg adsorbent, 150 mL sample volume, 5 min extraction time, 3 mL of 1:1 mixture of $\text{HNO}_3\text{+HCl}$ as desorption solvent with 1 min agitation time) for linearity, limit of detection (LOD), limit of quantification (LOQ), precision (repeatability and reproducibility) and accuracy (recovery). The results obtained are summarized in Table 1. Acceptable linearity from the linearity range of 20-100 $\mu\text{g/L}$ was obtained with good coefficient of determination ($R^2 = 0.974$). LOD (3 S/N) and LOQ (10 S/N) obtained were 1.70 $\mu\text{g/L}$ and 5.6 $\mu\text{g/L}$ respectively. The precision studies were

performed for one day ($n = 3$) and for three consecutive days ($n = 9$). Concentration of Cu(II) ion used was 100 $\mu\text{g/L}$. Satisfactory RSDs were obtained; 2.37% for repeatability and 5.15% for reproducibility showing good precision of the $\text{Fe}_3\text{O}_4\text{-CaAlg}$ MSPE method.

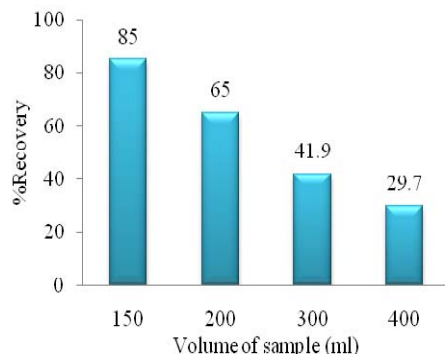


Figure 8: Effect of sample volume on % recovery of Cu(II) ions from water sample using $\text{Fe}_3\text{O}_4\text{-CaAlg}$ MSPE. Extraction conditions: 50 mg adsorbent; 5 min extraction time; Desorption conditions: 3 mL of 1:1 mixture of $\text{HNO}_3\text{+HCl}$ desorption solvent with 1 min agitation time

Table 1: Validation of $\text{Fe}_3\text{O}_4\text{-Ca Alg}$ MSPE for Cu(II) ion

Linear range ($\mu\text{g/L}$)	R^2	LOD ($\mu\text{g/L}$)	LOQ ($\mu\text{g/L}$)	Repeatability (\pm %RSD, $n = 3$)	Reproducibility (\pm %RSD, $n = 9$)
20-100	0.974	1.70	5.6	2.37	5.15

Application of the developed $\text{Fe}_3\text{O}_4\text{-Ca Alg}$ MSPE for Cu(II) ions from Tap and River Water Samples

In order to investigate the practicality of the proposed $\text{Fe}_3\text{O}_4\text{-CaAlg}$ MSPE method, it was applied to the analysis of Cu(II) ions in tap and Sungai Skudai water samples. For tap water sample, the concentration of Cu(II) ion was found to be 11.84 $\mu\text{g/L}$ while for river water sample, the concentration of Cu(II) ion found was 7.2 $\mu\text{g/L}$. Relative recovery studies were conducted by spiking tap water and river water samples to give a final concentration of 20 $\mu\text{g/L}$. Results showed that the relative recovery of tap water sample was 78.9% and for river water sample, 45.7% with RSDs $< 4.72\%$ ($n = 3$) for both (Table 2). The lower recovery of Cu(II) ions from the river water might be due to some external factor which affects the adsorption process such as the existence of cationic components in the river water sample as interferences. These components might compete with Cu(II) ions for the available adsorption sites thus decrease the extraction efficiency of Cu(II) ions (Paques et al., 2014). The alginate also may not be selective enough to adsorb Cu(II) ions in the complex sample. Besides, the pH of the river water sample should be taking into consideration as it may affect the extraction efficiency of metal ions. More acidic water sample contained more hydrogen ion which might also compete with the Cu(II) ion to adsorb onto the adsorbent.

Table 2: Relative recovery studies of Cu(II) ions from spiked tap and river water samples using the developed $\text{Fe}_3\text{O}_4\text{-CaAlg}$ MSPE method

Sample	Spiked level ($\mu\text{g/L}$)	Concentration of Cu(II) ions found ($\mu\text{g/L}$)	% Relative Recovery (\pm % RSD, $n = 3$)
Tap Water	0	11.84	-
	20	15.78	78.9 (4.72)
River Water	0	7.20	-
	20	9.14	45.7 (1.76)

CONCLUSION

The synthesised Fe₃O₄-CaAlg was successfully used as an adsorbent for Cu(II) ions using the developed MSPE technique. Acceptable linearity from the linearity range of 20-100 µg/L was obtained with good coefficient of determination ($R^2 = 0.974$). LOD of 1.70 µg/L and LOQ of 5.76 µg/L was obtained for Cu(II) ions. Good precision was obtained for the developed method (2.37% RSD ($n = 3$) and 5.15% RSD ($n = 9$)). The developed Fe₃O₄-CaAlg MSPE method was successfully applied to the analysis of tap water sample with good relative recoveries (78.9%) and RSD (4.72%) but lower relative recovery (45.7%, RSD 1.76%) for Cu(II) ions from river water which might be due to several external factors which affect the extraction efficiency. This shows that the developed MSPE method is sensitive to sample matrix. Further studies on parameters affecting recovery of Cu(II) ions such as pH of sample should be performed.

REFERENCES

- Bruce Fuhrer, A., & Dennis McHugh, B. J. (2003). *Cover photograph: Durvillaea potatorum on wave-swept rocks food and agriculture organization of the united nations*.
- Draget, K. I., Smidsrød, P. O., & Skjåk-bræk, P. G. (2005). Alginates from Algae, 1–30.
- Jana, Š., Andruš, V., Balogh, I. S., Kocúrová, L., Nagy, L., & Baze, Y. (2011). A novel, environmentally friendly dispersive liquid – liquid microextraction procedure for the determination of copper, **99**, 40–45.
- Ndlovu, T., Arotiba, O. a., Sampath, S., Krause, R. W., & Mamba, B. B. (2012). Electroanalysis of copper as a heavy metal pollutant in water using cobalt oxide modified exfoliated graphite electrode. *Physics and Chemistry of the Earth, Parts A/B/C*, **50-52**, 127–131.
- Paques, J. P., van der Linden, E., van Rijn, C. J. M., & Sagis, L. M. C. (2014). Preparation methods of alginate nanoparticles. *Advances in Colloid and Interface Science*, **209**, 163–71.
- Shrivastava, K., & Kumar, N. (2013). Dispersive liquid – liquid microextraction for the determination of copper in cereals and vegetable food samples using flame atomic absorption spectrometry. *Food Chemistry*, **141(3)**, 2263–2268.
- Wierucka, M., & Biziuk, M. (2014). Trends in Analytical Chemistry Application of magnetic nanoparticles for magnetic solid-phase extraction in preparing biological, environmental and food samples. *Trends in Analytical Chemistry*, **59**, 50–58.

KINETIC STUDY OF BIODIESEL USING EGG SHELL FOR BASE TRANSESTERIFICATION REACTION

Fatin Madihah binti Mamat and Abd Rahim Yacob

Department of Chemistry, Faculty of Science, Universiti Teknologi Malaysia, 81310 Johor Bahru

Abstract

The accumulative oil demands have produced a renewed interest in alternative fuels of biological origin. Alternative fuels, such as biodiesel has been focused unanimously because of current energy crisis. In this study, kinetics of heterogeneous transesterification of waste cooking oil (WCO) with prepared CaO-800 from the calcination of egg shell was discovered. Firstly, the egg shells were calcined at temperature of 800°C and 900°C. Then the catalysts were characterized using Thermal Gravimetry Analysis (TGA), Fourier Transformed Infrared (FTIR), Nitrogen Adsorption Analysis, Field Emission Scanning Electron Microscope (FESEM), and X-ray Powder Diffraction (XRD). The soluble basicity and the basic strength of the prepared catalysts were determined using back titration. The results showed that calcined egg shell at 800 °C was the most suitable catalyst to use in the biodiesel production as it had high basicity and high surface area compared to calcined egg shell at 900 °C. The product biodiesel prepared was then analyzed using Gas Chromatography- Flame Ionization Detector (GC-FID). The kinetic studies for the reaction was carried out at reaction time of 30, 60, 90, 120, 150 and 180 mins at temperature 45°C, 55°C, 65°C, 75°C and 85°C temperature respectively. The results showed that the reaction follows the zero order reaction, has the rate constant of 0.13 s⁻¹ and the activation energy is 23.2 kJ/mol.

Keywords: calcined egg shell, transesterification of waste cooking oil, biodiesel, kinetic study

INTRODUCTION

Biodiesel, long-chain fatty acid alkyl ester is one of the interesting alternative fuels which can be produced from renewable sources and provides complete combustion with less gaseous pollutant emission [1] The heterogeneous catalysts of alkaline earth metal oxides heteropolyacids and zeolites have been investigated for biodiesel production as they could be operated in continuous processes, could give high quality of products; they are reusable, environmentally and are more effective than acid catalysts and enzymes. Among these, alkaline earth metal oxides, and in particular CaO, have been shown to possess good performance of commercial significance for a wide spectrum of environmentally important reactions.

The biodiesel that were produced can be a renewable alternative to petroleum diesel and by using egg shell as catalyst we can reduce the production costs of biodiesel. Reuse of eggshell as catalyst for biodiesel production was investigated in the viewpoint of the recycle of eggshell waste, minimization of contaminants, reducing the production costs of biodiesel and making the process to produce biodiesel fully ecologically friendly.

Reaction kinetics is essential for reactor and process analysis, design, simulation and control. The previous research of the kinetic study for the transesterification of oil has been carried out for the alkali catalyzed reaction so this study will be carried out for based catalysed reaction.

EXPERIMENTAL

Materials

The chemical reagents used in this research were waste cooking oil, methanol, calcium oxide (CaO). The apparatus used are two-necked round bottom flask, measuring cylinder, hot plate stirrer, mortar and pestle, magnetic stirrer, thermometer, beaker, and retort stand.

Preparation of Egg Shell as Catalyst

The catalyst was prepared by the calcination of egg shell in electric furnace from temperature 800 °C to 900 °C. Firstly, the chicken egg shells were collected from cafeteria and washed with distilled water while the inner content of the egg shell were cleaned. The egg shells were washed again with distilled water, and dried using oven. The egg shells were crushed by using mortar and pestle until become powder and were calcined in an electric furnace from 800°C to 900 °C in 4 h.

Characterizations of Catalyst

The characterization of calcined egg shell has been carried out by using Thermogravimetric Analyzer (TGA), Fourier Transform Infrared (FTIR), X-Ray Diffraction (XRD), Field Emission Scanning Electron Microscopy (FESEM), Energy Dispersive X-Ray Spectroscopy (EDX), and N₂ Adsorption)

Base Heterogeneous Transesterification and Characterization of Biodiesel

A two-necked round bottom flask with a thermometer, a reflux condenser and magnetic stirrer were set up. A mixture containing of 0.1g prepared catalyst and 18.55g of purify methanol were heated 30 minutes with the temperature fixed at 65±5 °C and 20g of waste cooking oil was added into the round bottom flask. The biodiesel was distilled with temperature fixed at 65±5 °C to remove remaining impurities after cooled at room temperature. Then the mixture was centrifuged at 3000rpm for 10 minutes. The middle layer was extracted as biodiesel and was analyzed by using GC. The graphs of rate of reactions of biodiesel were plotted and the order of reaction was determined.

Characterization of biodiesel

The biodiesel that produced were characterized using Gas Chromatography - Flame Ionization Detector (GC-FID).The transesterification reaction for biodiesel production was recorded using a Hewlett Packed Gas Chromatography model 6890. The mobile phase used was helium gas and column DB-Wax with specification 0.25 µm thickness, 30 mm length and 0.20 mm internal diameter was used as stationary phase with Flame Ionization Detector (FID). Temperature conditions which applied in this research were oven temperature was set at initial value 40°C and hold for 3 min, increase to 195°C with the rate 25°C/min , subsequently the temperature rise up to 205°C with the rate 3°C/min and finally the temperature goes to 230°C with rate 8°C/min. For each temperature points, 5 min holding times was selected in order to complete the separation for each temperature settings. 10 mg heptanes in hexane was prepared, and 1 mL of this solution was added into 50 mg of sample. Then, 1 mL of this mixture was injected into GC.

The Kinetic Study

The kinetic study has been investigated to determine the order of reaction of the biodiesel by varied the temperature and time. The temperature and time were varied during the reflux process. The temperatures selected were at 45°C, 55°C, 65°C, 75 °C and 85°C while the time taken were 30 min, 60 min, 90 min, 120 min and 150 min.The graphs of rate of reactions of biodiesel were plotted using the percentage of conversion from the GC-FID results and the order of reaction was determined.

RESULTS AND DISCUSSION

In this study, biodiesel has successfully synthesized using the prepared calcined egg shell as catalyst and the order of reaction will be identified

Characterization of Catalyst

The characterization of calcined egg shell has been carried out by using Thermogravimetric Analyzer (TGA), Fourier Transform Infrared (FTIR), X-Ray Diffraction (XRD), Field Emission Scanning Electron Microscopy (FESEM), Energy Dispersive X-Ray Spectroscopy (EDX), and N₂ Adsorption

Thermal Gravimetry Analysis (TGA)

Figure 3.1 and 3.2 show the thermogram of egg shell and the Percentage of weight lost with different temperature regions. A few minor increasing of percentage of weight loss at temperature range of 0 to 250 °C was due to the removal of adsorbed water at the surface of egg shell sample. The major weight loss occurred at temperature range of 500 to 750°C with value of 10.2% was due to the removal of organic from the egg shell sample. Other related report indicated that the suitable temperature for the transformation of egg shell was in the range of 800 to 1000 °C .Therefore, in this study, it is expected that the complete transformation of egg shell occurs at temperature above 750 °C.

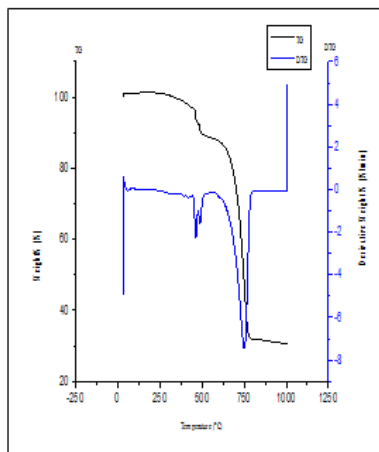


Figure 31: Thermogram of Egg Shell

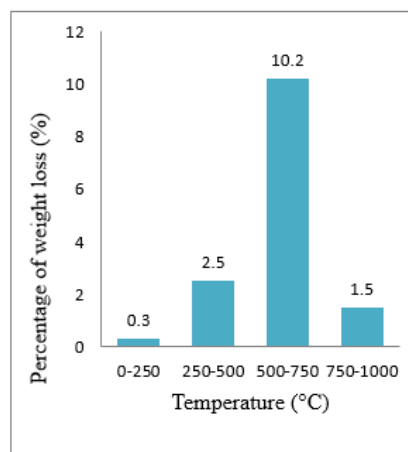


Figure 3.2: Percentage of weight lost with different temperature regions

Fourier Transform Infrared (FTIR)

Figure 3.3 and Table 1 show FTIR spectra of prepared a) CaO-800 and b) CaO-900 and summarization of peak assignment for (a) Ca-800 and (b) CaO-900. The egg shell starts to lose carbonate and produce CaO and carbon dioxide gas during calcination. The intensities of the peaks decrease related to CO_3^{2-} molecules (613 cm^{-1} , 950 cm^{-1} and 1500 cm^{-1}) was observed expect for CaO-800. This phenomenon occurred due to the reduction of the reduced mass of related functional group of CO_3^{2-} molecules. For CaO-800, the intense peaks appear at the wavelength of 950 cm^{-1} and 1500 cm^{-1} (C–O vibration) indicates that the majority compound present in the sample is CaCO_3 which may due to incomplete removal of CO_3^{2-} molecules. For CaO-900, the weak peaks for vibration modes of mono and bidentate carbonate shows that the sample contains impurities CaCO_3 with the reason of incomplete transformation. On the other hand, CaO-900 may contain higher purity of CaO due to less intense peaks for C–O vibration than CaO-800.

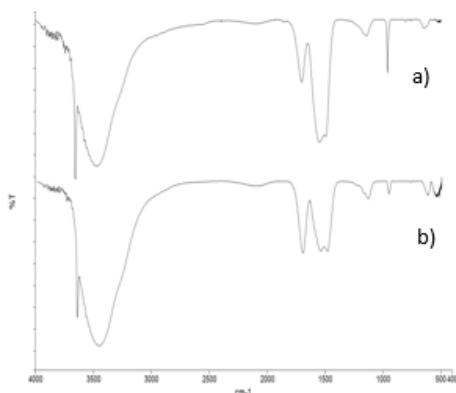


Figure 3.3: FTIR spectra of prepared a)CaO-800 and b) CaO-900

Wavelength (cm ⁻¹)	Peak Assignment
3640	O-H stretching vibration
3500	O-H stretching vibration
1650	O-H bending vibration
950 and 1500	C-O vibration modes
613	Lattice vibration CaCO_3
550	Ca-O symmetric vibration

Table1: Summarization of peak assignment for (a) Ca-800 and (b) CaO-900

X-Ray Diffraction (XRD) Analysis

Figure 3.4 shows that for CaO-900, diffraction reflections characteristics of calcite calcium carbonate, CaCO_3 was observed at $2\theta = 32.25^\circ$ while the peaks appear at 37.41° , 53.91° , 67.43° which displays diffraction reflections characteristics of portlandite calcium hydroxide, $\text{Ca}(\text{OH})_2$. The prepared catalyst calcined at 800°C ,

contains CaCO_3 as major component and $\text{Ca}(\text{OH})_2$ as minor component since the intensities of the peak of CaCO_3 at 32.21° is higher than the intensities of the peak of $\text{Ca}(\text{OH})_2$ at 28.62° . In contrast, the major component of prepared catalyst calcined at 800°C , CaO-800 was $\text{Ca}(\text{OH})_2$ while the minor component was CaCO_3 .

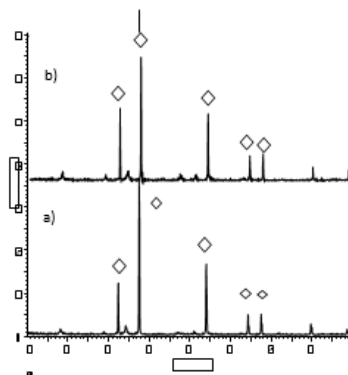


Figure 3.4: XRD Spectra of prepared a) CaO-800 and b) CaO-900

Nitrogen Gas Adsorption

As shown in Figure 3.5, an increase in specific BET surface area after calcination of egg shell (formation of CaO 800 and CaO-900) were observed where the BET surface area of CaO-800 was found to be $15.67\text{ m}^2/\text{g}$ while the BET surface area of CaO-900 was found to be $14.96\text{ m}^2/\text{g}$. This phenomenon may cause the appearance of defect sites on the surface of CaO-900 due to the decomposition of egg shell to CaO at the temperature of 900°C . This surface defects lead to an increase in catalytic activity of the reaction as the surface area of catalyst had been increased.

As CaO-800 with highest basicity and higher BET surface area had the most probably to exhibit higher catalytic activity for transesterification of waste cooking oil oil to produce biodiesel compared with CaO-900. This assumption is supported by basicity study and FESEM micrograph of the catalyst.

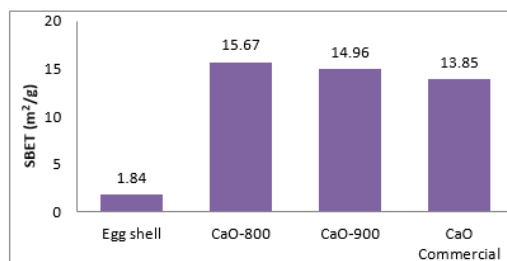


Figure 3.5: The specific SBET surface area of egg shell, CaO-800, CaO-900 and CaO commercial

Field Emission Scanning Electron Microscopy (FESEM)

Figure 3.7 and 3.8 demonstrate the surface morphology of CaO-800 and CaO-900 with magnification of 2.5 kX . From this study, CaO-800 comprises irregular shape of particles with various sizes due to the agglomeration of particles with each other. The surface of CaO-900 was not smooth. In addition, some wave-like surface and cracks on the surface which were not found over commercial CaO could possibly improve the surface area of CaO-900

Energy Dispersive X-Ray Spectroscopy (EDX)

From Figure 3.9, the prepared CaO-800 consists of major element which is calcium 72.67% and oxygen which are 24.98% respectively and some impurity elements were found such as Mg and C maybe because carbon

element had not completely removed from the sample by emission of carbon dioxide gas during calcination process while in figure 3.10 the prepared CaO-900 consists of major element which is calcium 54.74 % and oxygen which are 40.52 % respectively. The percentage of major element, calcium in CaO-900 is less compared to percentage of calcium in CaO-800 that was 72.67 %. That was the reason why CaO-800 was chosen as the catalyst in the transesterification of waste cooking oil.

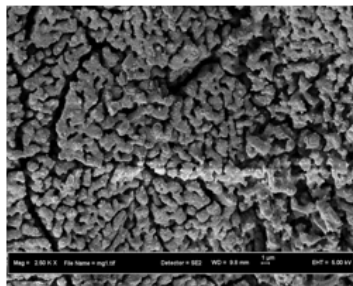


Figure 3.7: FESEM micrograph of CaO-800 with magnification of 2.5 kX

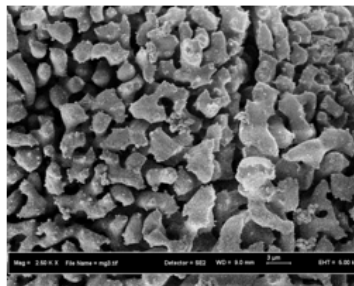


Figure 3.8: FESEM micrograph of CaO-900 with magnification of 2.5 kX

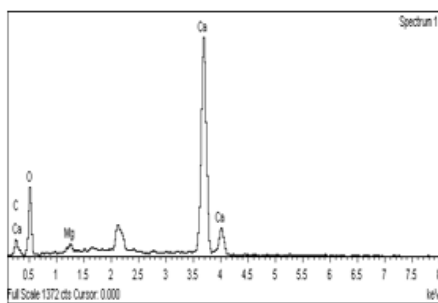


Figure 3.9: EDX Spectrum of CaO-800

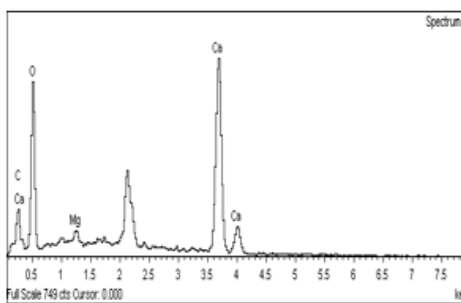


Figure 3.10: EDX Spectrum of CaO-900

Characterization of Biodiesel

The biodiesel, which is fatty acid methyl esters (FAMES), was analyzed by GC-FID in order to investigate the percentage conversion. Figure 3.11 shows an increase trend in percentage conversion of biodiesel as the reaction time increased. For 30, 60, 90, 120 and 150 minutes of reaction time, the percentage conversion of biodiesel were 67%, 75%, 78%, 82% and 83% respectively. It can be observed that as the reaction time increased, the percentage conversion or biodiesel yield also increased. It showed that the reaction time affect the yield of FAME while Figure 3.12 shows the increasing of percentage conversion of biodiesel when the temperature were increased. For temperature 45°C, 55°C, 65°C, 75 °C and 85°C, the percentage conversion were 36%, 47%, 81%, 83% and 85% correspondingly. When the reaction was carried out at 65°C, which is above the boiling point of methanol, the solvent vaporized and remained in the vapor phase in the reactor causing a reduction in the methanol in the reaction media.

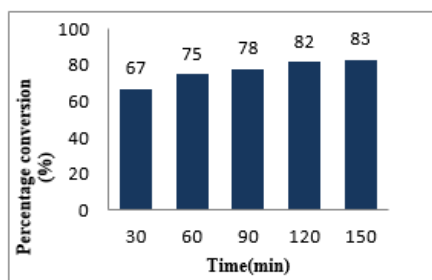


Figure 3.11: Percentage conversion of palm oil to biodiesel vs reaction time

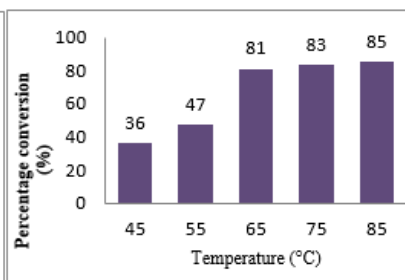


Figure 3.12: Percentage conversion of palm oil to biodiesel vs reaction temperature

The Rate of Reaction

Figure 3.13 shows the three graph of rate of reaction of (a) zero order (b) first order and (c) second order. R^2 obtained were 0.9163, 0.8946 and 0.7206 respectively. The R^2 of zero order was chosen as it was the highest R^2 and the rate constant was 0.13. The zero order signpost that rate of reaction apparently independent of the reactant concentration. The graph of $\ln K$ vs $1/T$ in Figure 3.14 below was plotted to determine the value of activation energy, E_a .

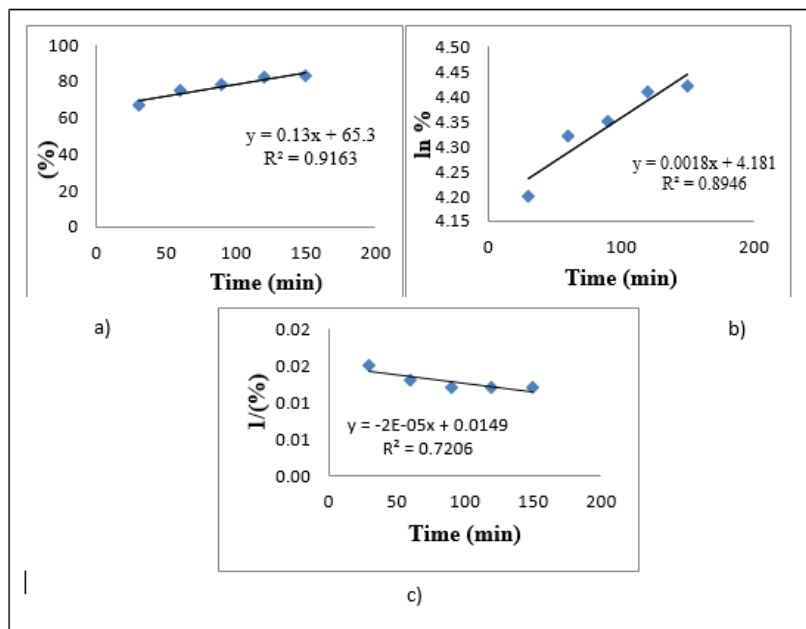


Figure 3.13: The rate of reaction of (a) Zero order (b) First order and (c) Second order

In Figure 3.14: Arrhenius plot for the calculated rate constants at the temperature of 45°C, 55°C, 65°C, 75°C and 85°C are presented. The slope define activation energy as a function of the reaction progress. The activation energy obtained was 23.2 kJ/mol. The activation energy which fall below the range of activation energy (26-82 kJ/mol) for heterogeneous transesterification reaction indicates that the reaction is not kinetic controlled

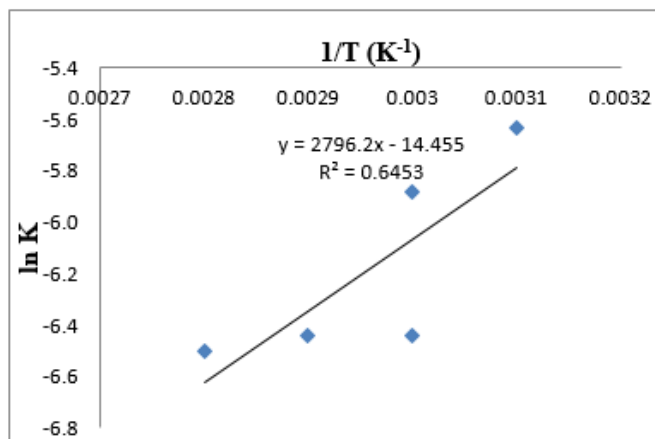


Figure 3.14 : Arrhenius law graph of zero order

CONCLUSION

In this study, calcium oxide that has been successfully prepared from the calcination process of egg shell at 800°C used to synthesize biodiesel. The kinetic reaction of transesterification reaction has been studied and the order of reaction has identified. The kinetic data used to optimize the process of biodiesel synthesis. From the high reaction rate obtained, the process proceeds via zero order and the activation energy obtained was 23.2 kJ/mol.

REFERENCES

1. N. Viriya-empikul a, P. Krasae b, W. Nualpaeng a, B. Yoosuk b, K. Faungnawakij. (2012). Biodiesel production over Ca-based solid catalysts derived from industrial wastes. *Fuel*, 239–244.
2. N. Viriya-empikul a, P. Krasae b, B. Puttasawat b, B. Yoosuk b, N. Chollacoop b, K. Faungnawakij a,* . (2009). Waste shells of mollusk and egg as biodiesel production catalysts. *Biosource Technology*, 3765-3768
3. Ziku Wei a,b, Chunli Xu a,b,*, Baoxin Li c. (2009). Application of waste eggshell as low-cost solid catalyst for biodiesel production. *Biosource Technology* **100**, 2883–2885.
4. Kawashima, A. Matsubara, K. & Honda, K. (2008). Development of heterogeneous base catalysts for biodiesel production. *Bioresource Technol.*, **99**, 3439–3443.

ESSENTIAL OIL OF *PIPER BETLE* AND DERIVATIVES OF EUGENOL

Rafidah Binti Husain and Farediah Binti Ahmad

Department of Chemistry, Faculty of Science, Universiti Teknologi Malaysia, 81310 Johor Bahru.

Abstract

The essential oil of *Piper betle* and the chemistry of its major compound have been investigated. The essential oil was obtained by hydrodistillation technique while the chemical compositions of the oil were determined by gas chromatography (GC), gas chromatography-mass spectrometry (GC-MS) and Kovats Indices. The yield of essential oil obtained from this plant was 0.64%. The compounds identified in the *P. betle* oil were six phenylpropanoids (40.38 %), three monoterpenes (0.15 %), and twenty one sesquiterpenes (38.95 %). Phenylpropanoids were the most dominant group in the oil of *P. betle* leaf with eugenol (32.64 %) being the main component. Eugenol was then separated from the oil by column chromatography and analyzed spectroscopically. The synthetic eugenol was subjected to methylation and acetylation to form methyl eugenol and eugenol acetate, respectively. The oil, eugenol and its derivatives were screened for antibacterial and antioxidant activities. For the antibacterial activity, only essential oil showed positive result at concentration of 900 ppm. While for the antioxidant activity, essential oil at IC₅₀ = 16.83 µg/mL and eugenol at IC₅₀ = 3.03 µg/mL, proved that both samples showed positive results on antioxidant assay.

Key Words: *Piperaceae*, *Piper betle*, eugenol, antioxidant, antibacterial

INTRODUCTION

The Piperaceae or also known as the pepper family is a large family of flowering plants consisting of 1,920 currently accepted species in 13 genera. The vast majority of peppers can be found within the two main genera which are *Piper* and *Peperomia*. Piperaceae species have been placed among the basal angiosperm and are adapted to a variety of habitats including moist forests, secondary vegetation and dry high lands [1]. This study was conducted on *P. betle* which is one of the members of Piperaceae family. *P. betle* is blessed as evergreen and perennial plant. Betle leaf has been described from ancient times as an aromatic, stimulo-carminative, astringent and aphrodisiac. The leaves are chewed with betel nut to improve the taste and to prevent halitosis [2]. The root have been used for treatment of cough, bronchial asthma, rheumatism, stomachalgia, edema of pregnancy and as contraceptive [3]. Consequently, the aim of this study was to evaluate the chemical compositions of the essential oil in the leaf and the chemistry of its major compound.

EXPERIMENTAL

Source of Sample

The sample of *P. betle* leaves were collected from Felcra Sungai Ara at Kota Tinggi. The leaves were washed and cut into small pieces.

Extraction and Analysis of Essential Oil

The fresh leaves (355 g) were placed in a round bottom flask (5 L) and covered with distilled water. The flask was equipped with a Dean Stark apparatus and water condenser and hydrodistilled for 10 hours. The mixture of oil and water in the Dean Stark was run off, extracted with Et₂O, dried over anhydrous MgSO₄ and filtered. The filtrate was left at room temperature for a few hours to evaporate the solvent. Evaporation of the solvent yielded *P. betle* oil (2.28 g, 0.64%) as a yellow liquid with pungent smell. The essential oil was analysed using GC chromatogram of the oil. Identification of the constituents was performed on the basis of their Kovats indices, which were calculated in relation to a standard hydrocarbon (C₆-C₂₆) and compared with those given in the literatures [4].

Isolation of Major Constituent

The essential oil (2.28 g, 0.64 %) was subjected to CC packed with SiO₂ (24.0 g). An eluent system consisted of a mixture of hexane and EtOAc of increasing polarity has afforded 135 fractions. Each fraction was monitored by TLC with hexane:EtOAc (90:10) as the developing solvent. Fractions with the same TLC

profiles were combined to give three new combined fractions. The fractions were labeled as F1 (0.047 g), F2 (0.196 g), and F3 (0.027 g). Fraction F3 was concentrated to yield eugenol (**1**) (0.027g, 1.20 %) as a yellow liquid; R_f 0.61 in (hexane:EtOAc/90:10).); IR (ATR) ν_{\max} cm^{-1} : 3516 (OH), 3077 (C-H sp^2), 2938 (C-H sp^3), 1638 (C=C olefinic), 1612 and 1431 (C=C aromatic), and 1264 (C-O); ^1H NMR δ (CDCl_3): 3.39 (2H, d, $J=6.8$ Hz, H-1'), 3.91 (3H, s, OCH₃), 5.18 (2H, m, H-3'), 5.85 (1H, s, OH), 6.04 (1H, m, H-2'), 6.76 (1H, dd, $J=8.4$ Hz and $J=2.0$ Hz, H-5), 6.94 (1H, d, $J=8.4$ Hz, H-6), 6.95 (1H, d, $J=2.0$ Hz, H-3); ^{13}C NMR δ (CDCl_3): 39.9 (C-1'), 55.9 (OCH₃), 111.1 (C-3), 114.3 (C-6), 115.6 (C-3'), 121.2 (C-5), 131.9 (C-4), 137.9 (C-2'), 143.9 (C-1) and 146.5 (C-2).

Chemical Modification of Eugenol (1)

Methylation

Eugenol (**1**) (0.10 g, 0.61 mmol) was mixed with CH_3I (0.15 g, 24.1 mmol) and K_2CO_3 (2.0 g) in acetone (10 mL) and refluxed for 10 h. The reaction mixture was then filtered and concentrated. The concentrated product was extracted with EtOAc (3 \times 10 mL). The combined EtOAc extracts was dried over anhydrous MgSO_4 , filtered and evaporated to dryness to give methyl eugenol as a yellow liquid (0.054 g, 53.8%) and R_f 0.60 (hexane:EtOAc/90:10). IR (ATR) ν_{\max} cm^{-1} : 3075 (C-H sp^2), 2936 (C-H sp^3), 1638 (C=C olefinic), 1511 and 1463 (C=C aromatic), 1260 (C-O); ^1H NMR δ (CDCl_3): 3.36 (2H, d, $J=6.8$ Hz, H-1'), 3.88 (3H, s, OCH₃), 3.89 (3H, s, OCH₃), 5.05 (2H, m, H-3'), 5.98 (1H, m, H-2'), 6.72 (1H, s, H-3), 6.83 (1H, d, $J=8.0$ Hz, H-5), 6.87 (1H, d, $J=8.8$ Hz, H-6). ^{13}C NMR δ (CDCl_3): 39.9 (C-1'), 55.8 (OCH₃), 55.9 (OCH₃), 111.3 (C-3), 111.9 (C-6), 114.2 (C-3'), 121.2 (C-5), 132.6 (C-4), 137.8 (C-2'), 143.9 (C-1) and 146.4 (C-2).

Acetylation

Eugenol (**1**) (0.1042 g, 0.61 mmol), acetic anhydride (0.1299 g, 1.24 mmol) and pyridine (0.1356 g, 0.062 mmol) were stirred overnight. The organic layer was extracted with CH_2Cl_2 (3 \times 5 mL) and dried over anhydrous MgSO_4 . The organic layer was then evaporated to dryness to give eugenol acetate (**3**) (0.0913 g, 87.6%) as a yellow liquid and R_f 0.62 (hexane:EtOAc/90:10). IR (ATR) ν_{\max} cm^{-1} : 3077 (C-H sp^2), 2939 (C-H sp^3), 1762 (C=O), 1638 (C=C olefinic), 1604 and 1508 (C=C aromatic), 1267 (C-O); ^1H NMR δ (CDCl_3): 2.32 (3H, s, CH_3COO), 3.39 (2H, d, $J=6.3$ Hz, H-1'), 3.83 (3H, s, OCH₃), 5.14 (2H, m, H-3'), 5.97 (1H, m, H-2'), 6.79 (1H, dd, $J=8.4$, and $J=2.4$, H-5), 6.81 (1H, d, $J=2.4$ Hz, H-3), 6.97 (1H, d, $J=8.4$ Hz, H-6). ^{13}C NMR δ (CDCl_3): 20.7 (CH₃), 40.1 (C-1'), 55.8 (OCH₃), 112.7 (C-3), 116.2 (C-3'), 120.7 (C-5), 122.5 (C-6), 137.0 (C-4), 137.9 (C-2'), 139.0 (C-1), 150.8 (C-2) and 169.3 (C=O).

Antibacterial Test

The tested microorganisms were Gram-positive and Gram-negative bacteria namely *Bacillus subtilis* ATCC 6633 and *Escherichia coli* ATCC 9027. The essential oil, eugenol (**1**), methyl eugenol (**2**), and eugenol acetate (**3**) were tested for antibacterial activity. Each sample was dissolved in DMSO to make 1.8 mg/mL stock sample. Disc of Streptomycin sulphate was used as the positive control while DMSO as the negative control. The McFarland reference was prepared by adding sulphuric acid (1% into broth nutrient) and hydrated barium chloride (1% into broth nutrient) (0.05 mL) in a covered vial and left at room temperature. The antibacterial tests were carried out through MIC (Minimum Inhibitory Concentration) and MBC (Minimum Bactericidal Concentration) method. The nutrient agar (20 g) and nutrient broth (8 g) were prepared by dissolved it with 1000 ml of distilled water. Then, the prepared solution were autoclaved for 2 hours 30 minutes at 50°C. The nutrient agar solution (5 mL) was pipetted into the agar plates. The agar plates were then kept in the refrigerator.

Antioxidant Activity

The essential oil, eugenol (**1**), methyl eugenol (**2**) and eugenol acetate (**3**) were measured for antioxidant activity by observing the change of purple colour solution of DPPH (diphenylpicrylhydrazyl). The sample solution was prepared by dissolving each sample (1 mg) in methanol (1 mL) to produce a concentration of 1000

ppm. The dilution from the stock solution were prepared in concentration of 100 ppm, 80 ppm, 60 ppm, 40 ppm, 20 ppm and 10 ppm. The purple colour solution of DPPH was prepared by dissolving DPPH (4 mg) in methanol (100 mL). The sample solution (100 μ L) was added to the DPPH solution (100 μ L) in a sample well. Sample which bleached the purple colour to yellow was considered active as DPPH radical scavenging.

RESULTS AND DISCUSSION

The Chemical Composition of Piper betle Oil

The GC and GC-MS analysis of this oil have been yielded thirty constituents. The compounds identified in the *P. betle* oil were six phenylpropanoids (40.38 %), three monoterpenes (0.15 %), and twenty one sesquiterpenes (38.95 %). Phenylpropanoid was the most dominant group in the oil of *P. betle* leaf with eugenol (**1**) (32.64 %) being the main component. Sesquiterpenes such as elemol (24.92 %), α -cadinol (4.97 %), γ -elemene (1.60 %), and Germacene D (2.43 %) were the most abundant constituents in *P. betle* leaf oil. While for monoterpenes, the compounds present in the oil were camphene (0.04 %), *cis*-ocimene (0.03 %), and linalool (0.08 %).

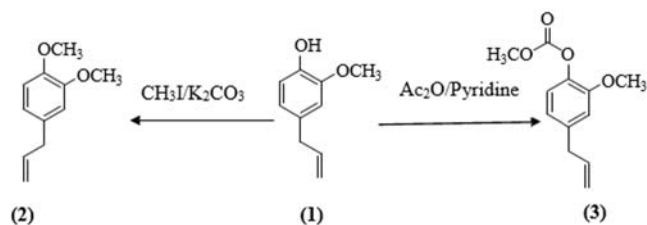
Chemical Constituents of Piper betle Leaf Oil

Eugenol (**1**) was isolated as a yellow liquid with a strong smell of clove. The TLC analysis displayed a single yellow spot with R_f value 0.61 in hexane:EtOAc (90:10). The IR spectrum showed a strong broad band at 3516 cm^{-1} , indicating the presence of hydroxyl group which was confirmed by an absorption band at 1264 cm^{-1} attributed to C-O. The bands at 1612 cm^{-1} and 1431 cm^{-1} were assigned as C=C of aromatic stretching, while the C=C olefinic stretching was represented by a band at 1638 cm^{-1} .

The ^1H NMR spectrum displayed two singlets at δ 3.91 and δ 5.85 corresponding to methoxyl and hydroxyl groups, respectively. The presence of an allylic side chain was confirmed by the signal resonance at δ 3.39 (2H, d, $J=6.8$ Hz), 5.18 (2H, m) and 6.04 (1H, m) corresponding to H-1', H-3' and H-2', respectively. The ^1H NMR spectrum also showed a doublet at δ 6.96, $J=2.0$ Hz attributed to aromatic proton H-3 while two mutual coupling aromatic proton of H-5 and H-6 were represented each by signal at δ 6.76 (dd, $J=8.4$ Hz and $J=2.0$ Hz), and δ 6.94 (d, $J=8.4$ Hz). The ^{13}C NMR spectrum showed the presence of 10 carbons with a methoxyl carbon at δ 55.9, and the aromatic carbons (C-3, C-5 and C-6) resonated at δ 111.1, δ 114.3 and δ 121.2, respectively. The three allylic carbons resonated at δ 39.9 (C-1'), δ 137.9 (C-2') and δ 115.6 (C-3'). The quaternary carbons, C-1, C-2 and C-4 were observed at δ 143.9, δ 146.5 and δ 131.9, respectively.

Chemistry of Eugenol (1)

Eugenol (**1**) was subjected to methylation, and acetylation reaction which resulted in methyl eugenol (**2**), and eugenol acetate (**3**).



Methyl Eugenol (2)

Methylation of eugenol with CH₃I in the presence of K₂CO₃ as base yielded methyl eugenol as a yellow liquid (0.054 g, 53.8% yield) and R_f 0.60 (hexane:EtOAc/90:10). The mild base, K₂CO₃ abstracted the hydrogen of the hydroxyl group to form the phenoxide ion which undergoes S_N2 reaction with methyl iodide to form (**2**). The IR spectrum of (**2**) exhibited the disappearance of OH absorption band at 3516 cm^{-1} . The ^1H NMR spectrum confirmed the formation of compound (**2**) by exhibiting two singlet signals at δ 3.88 and δ 3.89 corresponding to two methoxyl groups. In addition to this, the aromatic protons signals were observed at δ 6.72 (1H, s, H-3), 6.83 (1H, d, $J=8.0$ Hz, H-5) and 6.87 (1H, d, $J=8.8$ Hz, H-6). The ^{13}C NMR spectrum further

confirmed the success of methylation reaction by showing two signals at δ 55.8 and 55.9 attributed to two methoxyl groups.

Eugenol Acetate (3)

Treatment of eugenol (**1**) with acetic anhydride in pyridine has afforded eugenol acetate as a yellow liquid (0.0913 g, 87.6%) and Rf 0.62 (hexane:EtOAc/90:10). The IR spectrum of (**3**) showed the presence of an absorption band at 1762 cm^{-1} corresponding to an acetyl function. The presence of the acetyl group was further supported by the ^1H NMR spectrum which showed a singlet at δ 2.32 attributed to three protons of an acetyl group. The disappearance of hydroxyl signal at δ 5.85 for eugenol (**1**), have proved that the hydroxyl has been substitute by the acetyl group. The rest of the signals for protons were similar to eugenol (**1**). The ^{13}C NMR spectrum displayed a signal at δ 169.3 corresponding to a carbonyl group. Based on these data, (**3**) was characterised as 4-allyl-2- methoxyphenyl acetate or eugenol acetate. The mechanism occurred when pyridine as a nucleophile attacked the carbonyl of acetic anhydride to form the acetate and pyridinium ions. The acetate ion which acted as a base, abstracted a proton from eugenol (**1**) to produce the phenoxide ion. The phenoxide ion attacked the pyridinium ion followed by elimination of pyridine to form eugenol acetate (**3**).

Bioactivity studies of Piper betle

Antibacterial Test

Essential oil, eugenol (**1**), methyl eugenol (**2**) and eugenol acetate (**3**) were examined for antibacterial activity using MIC (Minimum Inhibitory Concentration) and MBC (Minimum Bactericidal Concentration) as the quantitative assays. The essential oil was found to have weak antibacterial activity against *B.subtilis* and *E.coli* with a concentration of 900 ppm. On the other hand, eugenol (**1**) and its derivatives, methyl eugenol (**2**) and eugenol acetate (**3**) were inactive towards the tested bacteria. It might due to the synergistic effect of the components presence in the essential oil contributed to the activity.

Antioxidant Assay

The rapid screening for antioxidant activity was performed on the essential oil, eugenol and its derivatives. DPPH or 1,1-diphenyl-2-picrylhydrazyl radical solution which was purple in colour and have a strong absorption at 517 nm was used for this assay. Sample which able to change the purple to yellow colour of DPPH is claimed to have active radical scavenger of DPPH as the molar absorptivity of DPPH radical at 517 nm decreased due to the odd electron of DPPH radical becomes paired with hydroxylated benzene to form the reduced DPPH-H. As a result, essential oil and eugenol was proven to have an antioxidant activities which the changes of the purple solution were observed. From the **Table 1**, IC₅₀ for the essential oil and eugenol were 16.83 $\mu\text{g/mL}$ and 3.03 $\mu\text{g/mL}$ respectively. Eugenol (**1**) had the lowest IC₅₀ value which is 3.03 $\mu\text{g/mL}$ compared to ascorbic acid with IC₅₀ = 10.83 $\mu\text{g/mL}$. It showed that eugenol is a potent antioxidant compared to ascorbic acid and the *P.betle* oil.

Table 1 : IC₅₀ values for the samples

Sample	IC ₅₀ ($\mu\text{g/mL}$)
Essential oil	16.83
Eugenol	3.03
Ascorbic acid	10.83

CONCLUSION

The hydrodistillation of fresh *P. betle* leaves afforded the essential oil (2.28 g, 0.64 %) as a yellow oil. The GC and GC-MS analysis of this oil have identified thirty constituents of six phenylpropanoids (40.38 %), three monoterpenes (0.15 %) and twenty one sesquiterpenes (38.95 %). A phenylpropanoid was found to be the main component in 32.64 % of eugenol (**1**). Camphene, cis-ocimene, and linalool were the compounds of

monoterpenes while elemol, α -cadinol, γ -elemene, and Germacene D represented the class of sesquiterpenes. Purification of the essential oil by column chromatography afforded the compound identified as eugenol (1). Methylation and acetylation of eugenol (1) produced methyl eugenol (2), and eugenol acetate (3) respectively. The essential oil, eugenol (1) and the derivatives were screened for antibacterial and antioxidant activity. For the antibacterial activity, only essential oil showed positive result at concentration of 900 ppm. While for the antioxidant activity, essential oil at $IC_{50} = 16.83 \mu\text{g/mL}$ and eugenol at $IC_{50} = 3.03 \mu\text{g/mL}$, proved that both samples showed positive results on antioxidant assay.

REFERENCES

1. Nikhil Kumar. (2010). Piper betle Linn. a maligned Pan-Asiatic plant with an array of pharmacological activities and prospects for drug discovery. *Current Science*. Vol. 99, No.7, 922-932.
2. Lin, C.-F., Hwang, T.-L., Chien, C.-C., Tu, H.-Y., & Lay, H.-L. (2013). New Hydroxychavicol Dimer from the Roots of Piper betle. *Molecules*, 18, 2563-25570.
3. Huang, X. Z., Yin, Y., Dai, J. H., Liang, H., Dai, Y., & Bai, L. (2009). Two New Ceramides from the Stems of Piper Betle L. *Chinese Chemical Letters*, 21, 433-436.
4. Robert P. Adams. (2007). Identification of Essential Oil Components by Gas Chromatography/Mass Spectrometry, 4th Edition. pg 804.

THE EFFECT OF PH ON THE FORMATION OF NICKEL NANOSTRUCTURES BY CHEMICAL REDUCTION METHOD

Mohd Ridhwan bin Ramdzan and Che Rozid bin Mamat

Department of Chemistry, Faculty of Science, Universiti Teknologi Malaysia, 81310 Johor Bahru

Abstract

The synthesis of nickel (Ni) nanostructures through chemical reduction method using hydrazine ($\text{N}_2\text{H}_4 \cdot 6\text{H}_2\text{O}$) as a reducing agent is reported. It was found the ratio of 6.65 of NaOH over NiCl_2 is necessary for the formation of pure nickel nanoparticles. NaOH was used to control the pH of solutions. Field Emission Scanning Electron Microscopy (FESEM) revealed that by varying $[\text{OH}^-]/[\text{Ni}^{2+}]$ molar ratio, various types of Ni nanostructures with size between 20 to 800 nm are obtained. Changing the pH from 8.7 to 9.5 resulted in formation of Ni wool-like nanostructure composed from chain-like nanostructure particles. The presence of nickel nanoparticles was confirmed with phase analysis using X-ray diffraction (XRD). Results show that the formation of pure Ni metal nanoparticles of wool-like nanostructure only occur when $[\text{OH}^-]/[\text{Ni}^{2+}]$ molar ratio was tailored to higher than four.

Keywords: chain-like, wool-like, nickel, nanostructures, nanoparticles

INTRODUCTION

Fascinating shapes and morphologies of nanoscale materials such as nanoparticles, nanorod, nanochain, nanocubes are among the most emerging classes of engineering materials due to its promising application in numerous technological and highly demanding fields such as sensing, biomedical, automotive, electronics, etc. [1-3]. Shape and size have been identified to have close relationship with chemical and physical properties of nanoscale materials. In some cases new properties are realized. The ability to produce nanoscale materials in various shapes and morphologies is becoming the key for further development of nanotechnology.

Pure bulk Ni is a lustrous white, hard and one of the four ferromagnetic elements at room temperature in transition metal group VIII of the Periodic Table. It has high ductility, good thermal conductivity, high strength and fair electrical conductivity. Ni nanoscale materials have received enormous attention due to their unique property in magnetic, thermal, electrical and chemical. It has been proven to have tremendous capability as catalyst, supercapacitor, additives in oil, magnetic carriers for biomedical and others [1,4-6]. Recently, synthesis of Ni in unique morphologies has becoming an interesting research because of the potential improvement of properties such as in chemical, electrical and magnetic. In some cases the new shape and morphologies create new properties which are differing when they are in spherical shape. Ni has been synthesized in various morphologies for instant, nanocubes, nanowires, flower-like, sea urchin-like and bowl-like [7-11].

In the synthesis of nanoscale materials, bottom-up approach is the most commonly used method. Bottom-up approach is a piecing together of system to a bigger system which usually involve chemical reaction such as wet chemical synthesis. Chemical reaction method has been extensively used as the synthetic method of producing nanomaterials with an advantage of more controllable of as-synthesized products. Utilizing this method, the preparation of nanoparticles can be achieved through various methods. Typical preparation chemical reaction method for Ni nanoscale materials includes polyol, microemulsion, microwave assisted and sol-gel [12-15]. Chemical reaction method requires consideration of several synthetic parameters for instant temperature, reaction time, reactants concentration etc. Wu et al. (2003) reported that Ni nanoparticles can only be obtained with appropriate amount of NaOH.

Ni nanostructure is structures that consist of Ni nanoparticles usually spherical in shape that self-assemble to form new structures. This unique phenomenon of self-assemblies, act differently depending on method of preparations. Under certain environment Ni nanoparticles tend to form secondary particles which are the results of van der Waals attractive forces and magnetic dipole interactions as well as thermodynamic driving force [17,18]. Different morphologies of nanoscale materials are normally associate with growth orientation direction. Chen et al. (2012) discovered that flower-like Ni structure is actually composed of sword-like petal particles that grows along (011) direction [19].

This work reports the effect of the pH to the shape and morphologies of as-synthesized particles by tailoring $[\text{OH}^-]/[\text{Ni}^{2+}]$ molar ratios using chemical reduction method. Investigation on the effect of pH on its shape and morphology will also be reported.

EXPERIMENTAL

Materials

All reagents are analytical grade and are used as received. Hydrazine hydrate 50% v/v, nickel chloride $\text{NiCl}_2 \cdot 6\text{H}_2\text{O}$ and sodium hydroxide powder NaOH are bought from Sigma- Aldrich company.

Preparation of Ni nanoparticles

To prepare the Ni nanoparticles, chemical reduction method of nickel salt (NiCl_2) by strong reducing agent, hydrazine hydrate in the aqueous solution are used due to better structural control on the microscopic level and low reaction temperature. The molar ratio of $\text{N}_2\text{H}_4/\text{Ni}^{2+}$ poured is 4.5 whereas that of $\text{NaOH}/\text{Ni}^{2+}$ is 2.66.

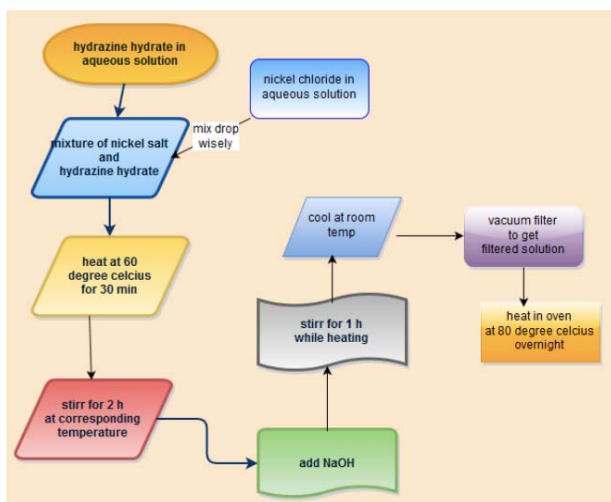


Figure 1: Process of synthesizing nickel nanoparticles product.

To be precise, 0.2 molar nickel chloride (NiCl_2) solutions are produced by diluting 0.5 g of nickel chloride solid salt with 10.517 mL of deionised water in a 25 mL beaker. 0.9 molar hydrazine hydrate (N_2H_4) are produced by diluting 2.12 mL N_2H_4 of 50% v/v concentration, 2.13 g cm^{-3} density, 40 g mol^{-1} with deionised water to make it 25 mL of solution in 50 mL beaker. The determining factor in producing nickel nanoparticle size is the amount of basic sodium hydroxide (NaOH) to alter reaction pH. 0.532 molar NaOH solutions are prepared by diluting 0.4 g NaOH powder with deionised water and are made to have 18.8 mL of NaOH solution in a 25 mL beaker. Second NaOH solution is made to increase NaOH power by 0.2 g to increase pH properties. The addition of 0.2 g NaOH powder is repeated for third, fourth and fifth solution.

NiCl_2 salt is mixed with deionised water in 50 mL beaker and shaken well. The salt solution is then put into 50 mL burette. Salt solution is poured drop wise from the burette into an appropriate amount of hydrazine hydrate (N_2H_4) taken into a flask of 250 mL. The solution of nickel salt and hydrazine hydrate are heated at 60°C for 30 min. The violet solution thus obtained is stirred for 2 h by using magnetic stirrer. An appropriate amount of NaOH is poured at corresponding reaction temperature and stirred again for an hour. The reduction reaction that takes place may be expressed by the following equation (Eq. 1).



The violet solution turned black in 10–15 min due to reduction reaction. The bluish- violet solution was obtained when the mixture of nickel chloride, NiCl_2 aqueous and hydrazine hydrate, N_2H_4 aqueous was heated for 30 min. The solution turns black when heated after the addition of sodium hydroxide, NaOH aqueous.



Figure 2: Bluish-violet solution

The resulting black coloured slurry is washed with deionised water repeatedly. The washing process is done in vacuum filtration filter filled with micron size filter paper before sucking process is done. The solid residue is vacuum filtered just after repeated washing with deionised water is done. Filtered nanopowder are placed in 1.5 L beaker and dried in the oven overnight at 80°C. Next day the dried powder is first crush into pieces using glass rod and taken into vial.

Characterization of Nickel nanoparticle

The particle sizes are determined by field emission scanning electron microscopy (FESEM) using a JEOL Model of JSM-6701F at 1nm (15kV) located at Institute of Ibnu Sina (IIS), Universiti Teknologi Malaysia Johor Bahru. FESEM is an ultra high resolution FESEM suitable for observation of fine structures of nickel nanoparticles.

XRD measurements are performed on a Bruker D8 Advance diffractometer which is licensed under Lembaga Perlesenan Tenaga Atom (LPTA) and is located in the Ibnu Sina Institute, Universiti Teknologi Malaysia Johor Bahru, using $\text{CuK}\alpha$ radiation ($\lambda = 0.1542 \text{ nm}$). The samples for XRD analyse is obtained by recovering the nickel nanoparticles from solution using a permanent magnet, then washing the precipitates using ethanol, and finally vacuum drying at room temperature.

RESULTS AND DISCUSSION

Formation of Ni nanoparticles

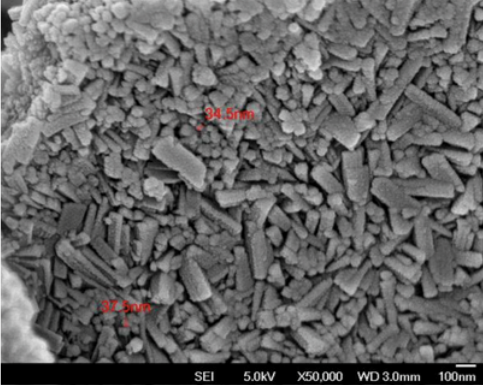
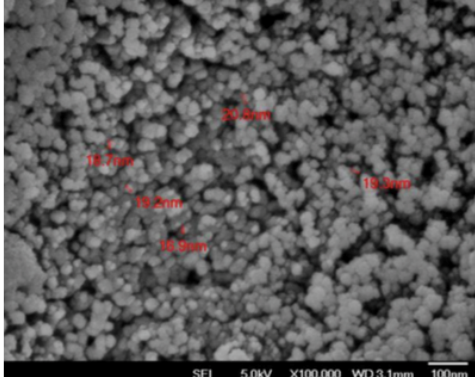
It is found that the addition of trace NaOH solution is necessary for the formation of pure nickel nanoparticles in an optimum reaction temperature of 60°C which is quite helpful in accelerating the reaction rate. It is found that the formation of nickel nanoparticles might be completed within 1 h at 60°C, but the reaction is not complete at 25 °C, even after 2 weeks. Therefore, the reaction temperature is set at 60-63°C in this work by using a digital hot plate to control the temperature.

The required molarity ratio of NaOH over NiCl_2 was raised from 2.66 to 6.65 by adding 1.0g of NaOH in the fourth trial as pH adjuster throughout the reduction reaction of nickel salt. The role of trace NaOH in the synthesis of Ni nanoparticles is quite interesting. The addition of trace NaOH led to the increase of solution pH from 8.7 to 9.5. It is suggested that the trace NaOH might act as a catalyst for the pure nanoparticle formation of nickel. Further investigation is necessary.

Particle size and structure Field emission scanning electron microscopy analysis (FESEM)

A typical FESEM micrograph and the size distribution for the nickel nanoparticles are shown in Table 4.1. Sample one(1) and four(4) having pH value of 8.7 and 9.5 respectively were characterized by FESEM at Institute of Ibnu Sina.

Table 1: FESEM structure and morphology sample 1 and 4.

Sample	Structure of nickel nanoparticle sample
1	
4	

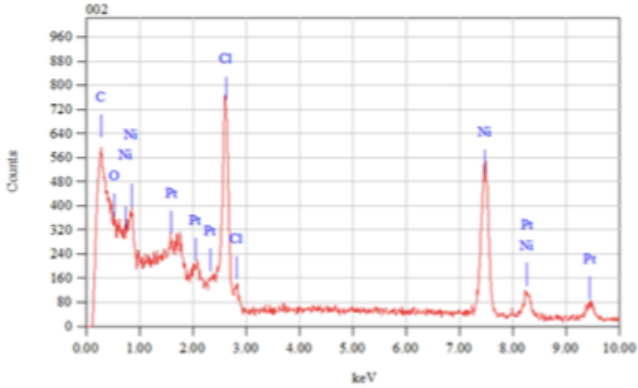
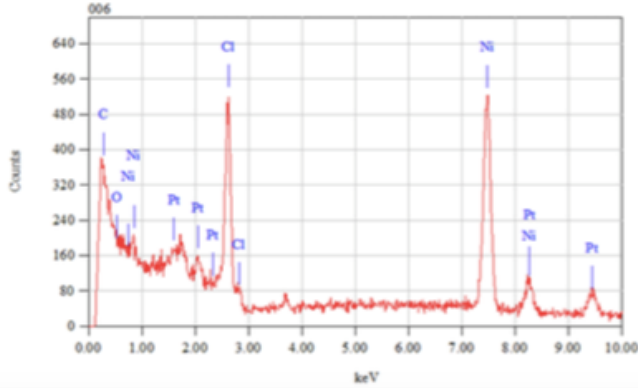
The effect of $\text{OH}^-/\text{Ni}^{2+}$ molar ratio on synthesized nanoparticles were investigated to study the effect on the reduction of Ni^{2+} ions, particles size distribution and morphology. FESEM micrographs of the particles obtained after reduction are shown in Table 1. The morphology of the starting $\text{Ni}(\text{OH})_2$ precursor (a) corresponds to long needle-like particles at 8.7 pH value. Upon reduction at higher pH value which is 9.5, the particle shape changed (b). This result correlates well with the XRD data, a clear indication that sample one(1) contains $\text{Ni}(\text{OH})_2$ precursor (i.e. elongated shape) while the Ni^0 nanoparticles is produced at higher pH value which is 9.5 for sample four(4) (i.e. round shape).

Besides, based on FESEM micrograph, higher molar ratio of $\text{OH}^-/\text{Ni}^{2+}$ of sample four(4) resulted in the formation of Ni^0 precursor with smaller size. Sample four(4) has an average particle size of 19 nm which is smaller compared to sample one(1) which having particles of 36 nm averagely. Thus, it can be concluded that higher pH value of the reaction cause the formation of smaller particles during reduction reaction.

Energy Dispersive X-ray analysis (EDX)

EDX analysis was performed for sample one(1) and sample four(4) having pH value of 8.7 and 9.5 respectively to analyse elemental composition in both samples. Peaks of elements in both sample can be seen in Table 2.

Table 2: EDX analysis of sample one(1) and sample four(4).

Sample	Structure of nickel nanoparticle sample
1	
4	

Based on EDX analysis shown above, nickel element is exist in both samples. The presence of other metal such as platinum is due to the coating purpose when doing sample preparation for FESEM and EDX analysis. Nickel counts for both sample is also the same due to the same amount of nickel chloride concentration used for nickel nanoparticles synthesis process.

The presence of chloride ion Cl^- can be observed at both samples in EDX analysis. But rather, chloride ion counts of sample four(4) is lower than sample one(1) which indicates the more successful in reduction reaction while sodium chloride, $NaCl$ solid is formed as a side product which then filter away by filter paper. Cl^- ion is still found in both sample is due to incomplete reduction reaction. This is believed due to the intensity of stirring process. The reduction reaction was performed with moderate stirring mechanism for all samples (intensity of 5 out of 10). Stronger stirring is needed to ensure complete reduction reaction. According to chemistry theory, more collision ensure better reaction which in this case is not that explain the existance of Cl^- ion in the sample.

X-ray diffraction analysis (XRD)

Sample one(1) of nickel nanopowder having 8.7 pH value is analysed by Bruker D8 Advance diffractometer using $CuK\alpha$ radiation ($\lambda = 0.1542$ nm) at 2θ in the range of 20° until 80° .

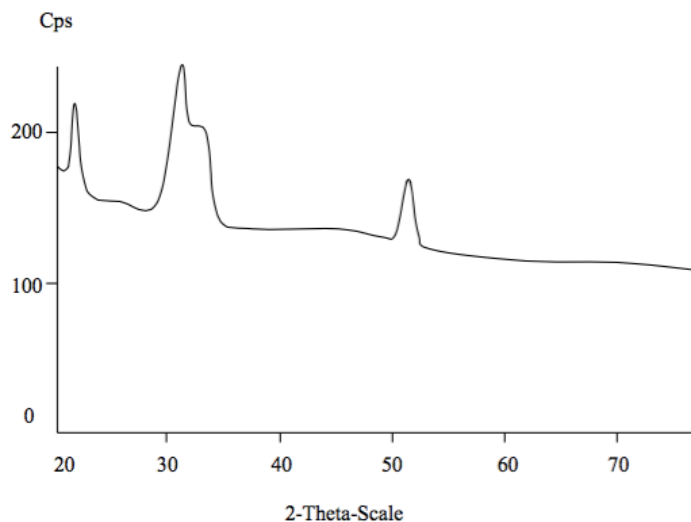


Figure 3: XRD peaks of sample one(1) at pH 8.7 (+0.0 g NaOH)

Based on the diffractogram shown above, major peaks are observed at around 21.948° and 31.337° which indicates the presence of Ni(OH)₂ precursor. Peak assigned to Ni⁰ is seen only at 51.093° having 200 crystal lattice structure.

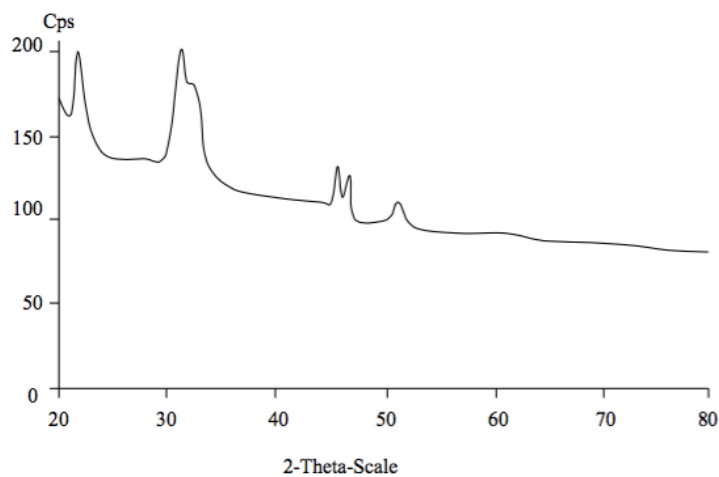


Figure 4: XRD peaks of sample four(4) at pH 9.5 (+0.6g NaOH)

Based on the spectrum above, major peaks are observed at around 21.943°, 31.235°, 32.510°, 45.445° and 51.275°. Ni(OH)₂ precursor are observed at 21.943°, 31.235° and 32.510° which are quite similar with peaks observed at sample one diffractogram. On the other hand, the peaks assigned to Ni⁰ precursor are observed for sample four(4) at diffraction line of 45.445°, 51.275°. Pure Ni⁰ was the only product observed for sample four(4), thus indicating that the reduction process leading to the formation of Ni⁰ requires higher NaOH/Ni²⁺ molar ratio.

Better Ni⁰ precursor was found in sample four(4) having 111 lattice structure. Ni⁰ precursor having 200 lattice structure is also observed in sample four(4). As a conclusion, higher pH value in sample four(4) leads to the formation of Ni⁰ precursor having 111 lattice structure. Ni⁰ precursor at 45.445° is better than Ni⁰

precursor at 51.275° due to the fact that 111 structure is higher in surface area. This criteria provide higher activity in term of catalysis in application scope.

Effects of sodium hydroxide on nickel nanoparticle crystal formation

Base on XRD spectra between sample one(1) and four(4), it is found that the addition of trace NaOH solution is necessary for the formation of pure nickel nanoparticles and an elevated reaction temperature of maximum 60oC is quite helpful in accelerating the reaction rate. It is found that the formation of nickel nanoparticles is completed within 1 h at 60oC, but the reaction is not complete at 25°C, even after 2 weeks. No nickel nanoparticle formation will happen even after one month of heating at 25°C.

Besides, adding extra NaOH molarity affect the formation of nickel nanoparticles precursor. This can be observed on the differences of sample four(4) and sample one(1) diffractograms. Sample four(4) contain diffraction lines of Ni⁰ precursor while non is observed on sample one(1) diffractogram. It can be concluded that NaOH plays an important role in forming pure nickel nanoparticle formation and also as pH adjuster throughout the reaction.

CONCLUSION

Nickel nanoparticles have been synthesized by the hydrazine reduction of nickel chloride at 60°C without soluble polymer as a protective agent. It is found that the addition of trace NaOH is necessary to form pure nickel nanoparticles precursor. The resultant particles have been characterized to be nickel amorphous structure by XRD. Nickel nanoparticle size is observed by FESEM to be around 36nm in sample one while 20 nm in sample four. The determining factor is the molarity of NaOH which identify NaOH is crucial to enhance the reaction rate thus forming difference nanostructures at difference pH. At 9.5 pH value of higher NaOH/Ni²⁺, FESEM reveals the existance of 111 Ni⁰ precursor. Stirring intensity also affect the reduction reaction in producing nickel nanoparticles.

REFERENCES

1. Stixrude, Lars; Wasserman, Evgeny; Cohen, Ronald (November 1997). "Composition and temperature of Earth's inner core". *Journal of Geophysical Research (American Geophysical Union)* 102 (B11): 24729–24740.
2. Derek G. E. Kerfoot (2005), "Nickel", *Ullmann's Encyclopedia of Industrial Chemistry*, Weinheim: Wiley-VCH, doi:10.1002/14356007.a17_157
3. Kittel, Charles. (1996). *Introduction to Solid State Physics*. Wiley. p. 449.
4. Keith Lascelles, Lindsay G. Morgan, David Nicholls, Detmar Beyersmann "Nickel Compounds" in *Ullmann's Encyclopedia of Industrial Chemistry 2005*, Wiley-VCH, Weinheim. doi:10.1002/14356007.a17_235.pub2
5. Greenwood, Norman N.; Earnshaw, Alan (1997). *Chemistry of the Elements* (2nd ed.). Butterworth-Heinemann. ISBN 0080379419.
6. Kuck, Peter H. "Mineral Commodity Summaries 2012: Nickel" (PDF). United States Geological Survey. Retrieved November 19, 2008.
7. Kuck, Peter H. "Mineral Yearbook 2006: Nickel" (PDF). United States Geological Survey. Retrieved November 19, 2008.
8. Davis, Joseph R (2000). "Uses of Nickel". *ASM Specialty Handbook: Nickel, Cobalt, and Their Alloys*. ASM International. p. 7–13.
9. Keith Lascelles, Lindsay G. Morgan, David Nicholls, Detmar Beyersmann "Nickel Compounds" in *Ullmann's Encyclopedia of Industrial Chemistry 2005*, Wiley-VCH, Weinheim.
10. Baucom, E. I.; Drago, R. S. (1971). "Nickel(II) and nickel(IV) complexes of 2,6- diacetylpyridine dioxime". *Journal of the American Chemical Society* 93 (24): 6469.
11. Mond, L.; Langer, K.; Quincke, F. (1890). "Action of carbon monoxide on nickel". *Journal of the Chemical Society* 57: 749–753.
12. Faraday, M. (1857) *Philos. Trans. R. Soc. London* , 147 , 145 – 181.
13. Turkevich, J., Stevenson, P.C., and Hillier, J. (1951) *Discuss. Faraday Soc.* 11, p. 55 – 75.
14. Rheenen, P.R.V., McKelvy, M.J., and Glaunsinger, W.S. (1987) *J. Solid State Chem.* 67, p. 151–169.
15. Henglein, A. (1989) *Chem. Rev.* , 89 , p. 1861 – 1873.
16. Burda, C., Chen, X., Narayanan, R., and El-Sayed, M.A. (2005) *Chem. Rev.* , 105 , p. 1025 – 1102.
17. Liz-Marzán, L.M. (2006) *Langmuir* , 22 , p. 32 – 41.
18. Sugimoto, T. (2000) *Fine Particles: Synthesis, Characterization, and Mechanisms of Growth*, *Surfactant Sci. Series Vol. 92*, Marcel Dekker Inc., New York.
19. Lea, M.C. (1889) *Am. J. Sci.*, 37, p. 476 – 491.

20. Yamaguchi, Y. (2008) Kagakukougaku, 72, p. 344 – 348.
21. Stoeva, S., Klabunde, K.J., Sorensen, C.M., and Dragieva, I. (2002) J. Am. Chem. Soc., 124, p. 2305 – 2311.
22. Lee, S.C. (2005). Synthesis, Characterisation and Catalytic Properties of Titanium Containing Silica Aerogel. Universiti Teknologi Malaysia: Master thesis.
23. Zainal Arifin et. al. (2001). Workshop on qualitative XRD phase identification. School of Material & Mineral Resources Engineering, Engineering Campus, Universiti Sains Malaysia. p. 1-11.
24. Ekhsan, J. (2009). Effect of titanium loading on physical properties and catalytic performance of phosphate-vanadia impregnated silica. Universiti of Teknologi Malaysia: Bachelor Thesis.
25. Parida, K. M., Sahu, N., biswal, N. R., Naik, B., Prandhan, A. C. (2008). Preparation, characterisation and photocatalytic activity of sulphate-modified titania for degradation of methyl orange under visible light. Journal of Colloid and Interface Science. 318. p. 231-237.

HYDRATION AND PROPERTIES OF BLENDED CEMENT SYSTEM INCORPORATING AEROGEL

Mohd Ikram Nul Hakim Bin Baharom and Che Rozid Bin Mamat

Department of Chemistry, Faculty of Science, Universiti Teknologi Malaysia, 81310 Johor Bahru.

Abstract

The utilization of supplementary cementing materials (SCMs) to produce economical cement that is cheaper and greener is an ongoing issue. The objectives of this study are to determine the effect of SCMs on the hydration and properties of blended cement. In this study, OPC was improvised by addition of GGBS and RHA with different weight percentages. Both types of respective were added with 1%, 2% and 3% of aerogel to improve its strength and hydrated for 7 and 28 days. The specimens were characterized by using compressive strength test, FTIR, FESEM, XRD and TGA techniques. The compressive strength test shows all specimens have increase in strength for 7 and 28 days in which the composition of OPC-GGBS with 1% aerogel shows the highest compressive strength at early hydration. FTIR shows the functional group present in the OPC- GGBS-Aerogel and OPC-RHA-Aerogel blended cement which are the water lattice of CH, CSH and CASH. The hydration product formed such as CH, CSH and ettringite were observed by using FESEM having plated shaped, foil honey-comb and fine needle-like crystal structure respectively. The formation of the hydrated was confirmed by XRD technique. The TGA technique indicates that there were 3 stages of percentage decomposition of weight loss occur on both type of specimens associated with aerogel.

Keywords: SCM, GGBS, RHA

INTRODUCTION

Cement have many properties that contribute to its strength setting and quality. These properties is assessed and control by measuring the parameter involved such as compressive strength of cement , surface area, particle size distribution, fineness and mineral composition. The production of cement is very expensive nowadays. The rapid growth in construction industry increase the demand on cement production. The cement industry is considered to be one of the most energy consuming industries, with a high rate of carbon dioxide (CO₂) emissions. Every year, it is responsible for approximately 5% of the global manmade CO₂ emissions [1]. Supplementary cementing materials (SCMs) is a proven material addressing a climate change and clean air. SCMs can be divided into natural materials and artificially made which both exhibit cementitious properties [2-3]. Some of these materials are called pozzolans (natural), which by themselves do not have any cementitious properties, but when used with portland cement, react to form cementitious compounds. Artificial SCMs have been investigated before, such as fly ash, rice husk ash, and silica fume. Their utilization has been an interesting subject of research for economic, environmental and technical reasons. When different material replaced, each materials possess different chemical and mineralogical compositions as well as different particle characteristics that have various effect on the properties of cement and concrete [4].

EXPERIMENTAL

Materials

The material that used in this study were Type 1 OPC, manufactured by Tasek Cement Corporation Berhad with 340 m²/kg specific surface. GGBS with 465 m²/kg specific surface area manufactured by YTL Cement Berhad. RHA that have been burn at 650-700 °C with excess air. Aerogel was synthesized by sol gel method followed by supercritical carbon dioxide drying.

Characterization of Blended Cement

Compressive Test Machine

The mixture of different composition blended cement were prepared by 50 mm x 50 mm x 50 mm cubes. The compressive strength test was done in accordance with ASTM C109/C109M [35]. After 24 hours, the test specimens were demolded and then cured in water. Three cubic test specimens were made from each mixture, covering two different ages of 7 and 28 days.

X-Ray Diffraction (XRD)

Phase purity and crystallinity of the samples were determined by XRD using a powder diffractometer with Cu K_{α} as the radiation source with $\lambda = 1.5418\text{\AA}$. The X-ray tube voltage and current were fixed at 40 kV and 40 mA, respectively. The scan step size was 2θ in the range from 5° to 80° and the reflection position and δ -spacing were calculated from the raw data using automated data analysis programs.

Fourier Transform Infrared Spectroscopy (FTIR)

KBr technique was used. About 1/100 of sample to KBr ratio was taken by using microspatula and teaspoons respectively. Next mix both thoroughly in a mortar while grinding with the pestle. A force of approximately 10 ton was applied under vacuum for 2 minutes to form transparent pellet. Then, the pellet formed was inserted in the pellet holder and go into the sample chamber. Lastly the measurement was performed and the IR spectra was observed.

Field Emission Scanning Electron Microscope with Energy Dispersive X-ray spectroscopy (FESEM-EDX)

FESEM equipped with energy dispersive X-ray spectroscopy (EDX) was used to analyze the surface morphology and elemental information of the cement paste. A small fractured sample was soaked in acetone to stop hydration and dried at 80°C for 2 h. Then the sample was coated with 20 nm of gold to make it conductive. The accelerating voltage was set at 10 kV.

Thermogravimetry Analysis (TGA/DTA)

The percentage decomposition OPC-GGBS-aerogel and OPC-RHA aerogel for 28 day was determined using TGA/DTA. The parameter used to operate the TGA was heating rate $20^{\circ}\text{C}/\text{min}$ under nitrogen atmosphere. The temperature range was $50\text{-}900^{\circ}\text{C}$.

RESULTS AND DISCUSSION

Compressive Strength Test

The compressive strength of cement paste containing OPC-GGBS-aerogel 1% was greater than others composition due to the high pozzolanic reaction at early age. But when compared to control mix at 28 days the strength of other mix was lesser, this decline was result of low pozzolanic reaction of the SCMs

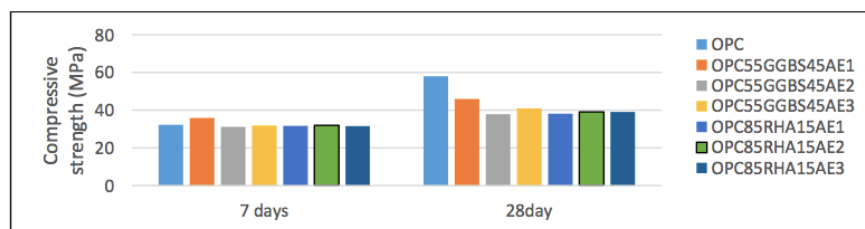


Figure 1 : Compressive strength development for 7 and 28 days

Determination of functional group in blended cement

The broad bands located at 3434 cm^{-1} and 1643 cm^{-1} are assigned to the stretching and bending vibrations of water lattice in CSH, CAH and hydrated calcium sulfoaluminates (CASH) hydrates. The band that appeared around 970 cm^{-1} is attributed to CSH.

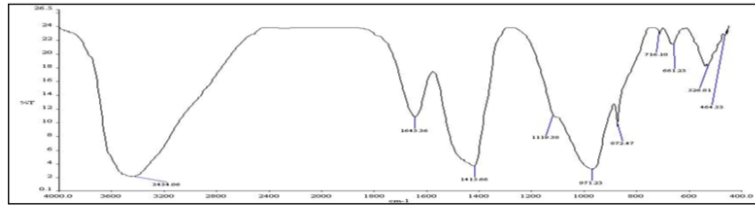


Figure 2 : FTIR spectra of OPC-GGBS-Aerogel 1%

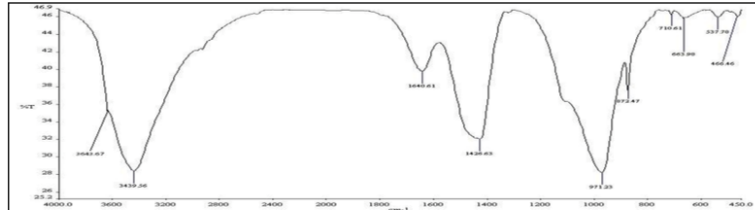


Figure 3 : FTIR spectra of OPC-RHA-Aerogel 2%

Morphology Characteristic

There were great deals of plated shaped of CH (a) formed at 28 day. A foil honey-comb structure of CSH are present in the micrograph (b). It is indicate that the hydration reaction occurring. Some of the hydrated product are still surrounded by fine needle-like crystal which reveal a clear improvement in the performance characteristic of cement paste in (d). A large hexagonal shaped crystal CH present that contribute to higher strength in (e)

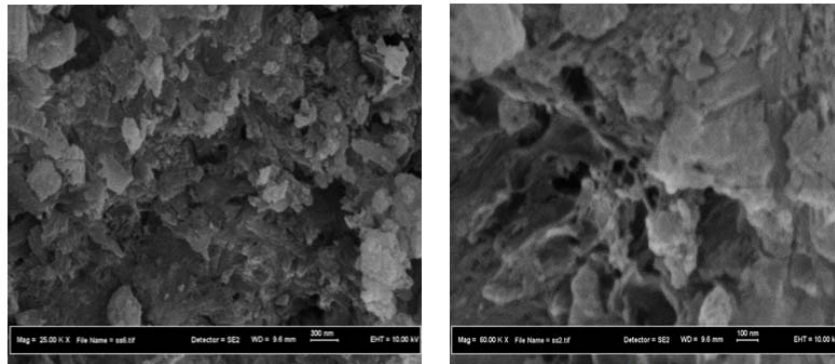


Figure 4 : (a) and (b) FESEM images of OPC-RHA-Aerogel 2% at 28 days

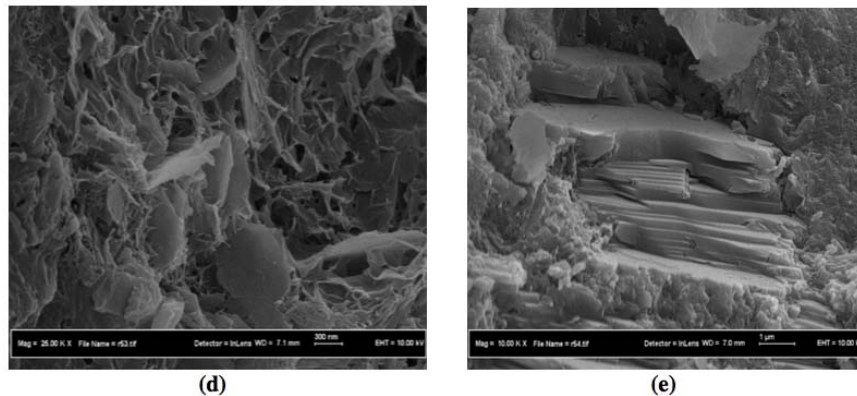


Figure 5 : (d) and (e) FESEM images of OPC-GGBS-aerogel (1%) at 28 days

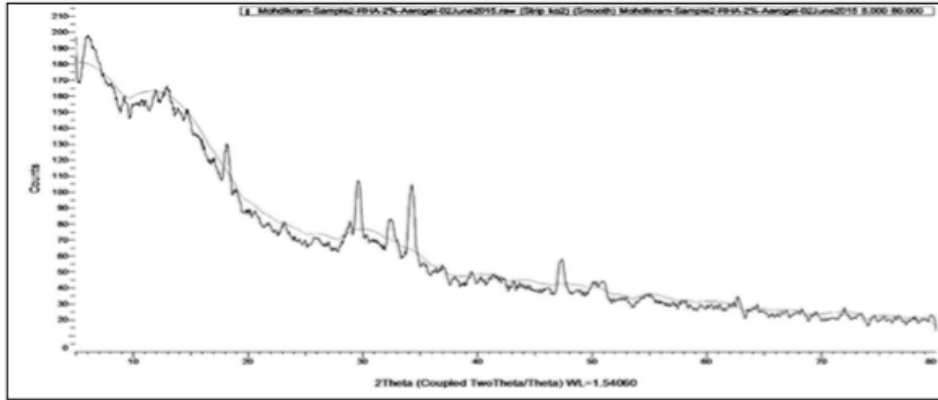


Figure 6 : OPC-RHA-Aerogel 1%

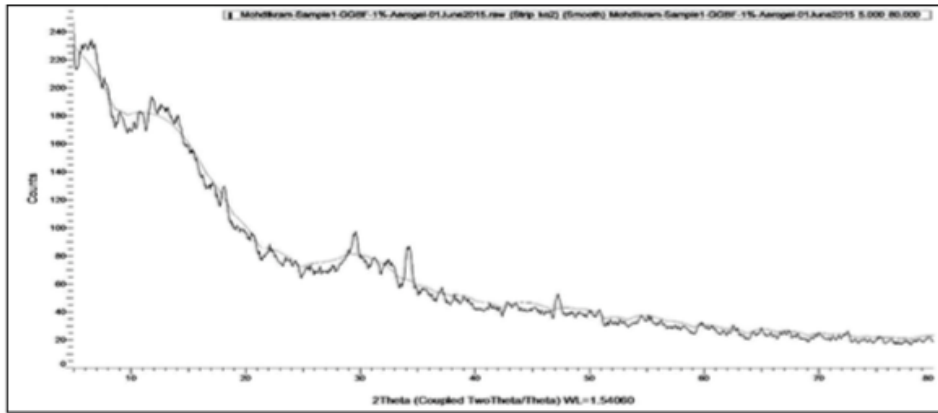


Figure 7 : OPC-GGBS-aerogel 1%

Calcium hydroxide, also known as portlandite (CH), presented at 34.259°, 18.133°, 47.358° and 34.213°, 18.133°, 47.282° in Figure 6 and Figure 7 respectively. The low intensity peak of CH in Figure 7 is due to pozzolanic reaction of the active silica and alumina of the GGBS during hydration to form CSH.

Percentage decomposition of blended cement

The first weight loss for OPC-GGBS-Aerogel 1% was lower than OPC-RHA-Aerogel 2% by 2.51%. This indicate that the amount hydrated product like water, ettringite or CSH was higher. The second weight loss is due to the decomposition of CH. Based on the table, OPC-GGBS- Aerogel 2% has the highest weight loss that is 2.74% that can relate to its strength. Due to the low third weight loss, it can be proved that OPC-RHA-Aerogel 2% has carbonate ion but the amount was low.

Table 1 : Weights loss of sample

Sample	Weight Loss (%)			
	First	Second	Third	Total
OPC-GGBS-Aerogel 1%	21.24	2.74	0.87	24.85
OPC-RHA-Aerogel 2%	23.75	1.86	0.28	25.89

CONCLUSION

The uses of SCMs have been experimentally proven to give some effect on the blended cement paste. In this study, OPC have been partially substituted with GGBS and RHA which the percentage of aerogel for both specimen were 1%, 2% and 3%. The sample were characterized by using variety of instruments. From the compressive strength test, all the specimen have increase in strength with curing time. OPC-GGBS-Aerogel 1% has higher strength at early hydration than other mix. Based on the IR spectrum, the main bands located at 3440 cm^{-1} and 1640 cm^{-1} related to the stretching and bending vibrations of water lattice in CSH, CAH and CASH.

Another main band appeared around 970 cm^{-1} which attributed to the present of CSH. It is observed from the spectrum that the hydration product are formed. In FESEM images, the structure of hydration product observed. At 28 days, a fine needle-like ettringite was observed followed by hexagonal plate-like crystal that is CH or portlandite. The CSH structure was present as foil honey-comb. In the XRD pattern fine crystalline formation was observed that are CH, CSH and C₃S. Based on the weight loss from TGA, there are 3 main decomposition occur with first decomposition are continuous weight loss start at 100-300°C followed by 450-550°C and lastly 650-900°C. CH decomposition start in the range of 450–550°C. It is proven that GGBS, RHA and addition of aerogel has pazzolanic effect in the cement paste which provide positive result on physical properties of the blended cement.

REFERENCES

1. Shen, L., Gao, T., Zhao, J., Wang, L., et al. (2014). Factory-level measurements on CO₂ emission factors of cement production in China. *Renewal. Sustainable. Energy Reviews.* 34, 337–349.
2. V. G. Papadakis, S. Tsimas. (2005). Greek supplementary cementing materials and their incorporation in concrete. *Cement & Concrete Composites.* 27, 223–230.
3. V. G. Papadakis, S. Tsimas. (2002). Supplementary cementing materials in concrete Part I: efficiency and design. *Cement and Concrete Research.* 32, 1525–1532.
4. S. Targana, A. Olgunb, Y. Erdoganb, V. Sevinc. (2002). Effects of supplementary cementing materials on the properties of cement and concrete. *Cement and Concrete Research.* 32, 1551–1558.

ISBN 978-967-0194-52-3



9 789670 194523

PROCEEDINGS Chemistry Undergraduate
Final Year Project Symposium 2014/2015
@ Published by Department of Chemistry
Faculty of Science, Universiti Teknologi Malaysia